

A Phase Transition between Positional and Semantic Learning in a Solvable Model of Dot-Product Attention

Hugo Cui¹, Freya Behrens¹, Florent Krzakala², and Lenka Zdeborová¹

¹Statistical Physics Of Computation laboratory, EPFL, Switzerland

²Information Learning & Physics laboratory, EPFL, Switzerland

{hugo.cui, freya.behrens, lenka.zdeborova, florent.krzakala}@epfl.ch

Abstract

We investigate how a dot-product attention layer learns a positional attention matrix (with tokens attending to each other based on their respective positions) and a semantic attention matrix (with tokens attending to each other based on their meaning). For an algorithmic task, we experimentally show how the same simple architecture can learn to implement a solution using either the positional or semantic mechanism. On the theoretical side, we study the learning of a non-linear self-attention layer with trainable tied and low-rank query and key matrices. In the asymptotic limit of high-dimensional data and a comparably large number of training samples, we provide a closed-form characterization of the global minimum of the non-convex empirical loss landscape. We show that this minimum corresponds to either a positional or a semantic mechanism and evidence an emergent phase transition from the former to the latter with increasing sample complexity. Finally, we compare the dot-product attention layer to linear positional baseline, and show that it outperforms the latter using the semantic mechanism provided it has access to sufficient data.

1 Introduction

Recent years have seen an upheaval in our ability to learn and implement complex tasks from textual data. Central in these advances is the use of self-attention layers (Vaswani et al., 2017), which provide an efficient method of extracting information from sentences – both the information encoded in the ordering (i.e. *positions*) of the words, and that encoded in the meaning (i.e. *semantics*) of the words. In theory, attention mechanisms are able to leverage both types of information, by having tokens attend to each other based on their respective positions (called positional attention in (Jelassi et al., 2022)) and/or respective meanings (henceforth referred to as semantic attention).

We aim to expand the up-to-now rather scarce theoretical understanding of learning with attention layers. Seminal open questions include: To what extent do transformers learn semantic or positional attention matrices? How does this depend on the amount of available data, the task, or the type of embedding? The present manuscript explores these questions, by proposing and analysing a solvable model of dot-product attention that can learn to implement both positional and semantic attention mechanisms from data. In particular our contributions are:

- We first illustrate how, for the histogram task, two qualitatively different solutions exist in the same loss landscape of a simple transformer, respectively corresponding to positional and semantic attention.
- We then move on to describe a model with a single self-attention layer with tied, low-rank query and key matrices. On Gaussian input data and realizable outputs, we show that this model exhibits a phase transition in terms of sample complexity between a semantic and positional mechanism.
- For this model, in the asymptotic limit where the embedding dimension d of the tokens and the number n of training samples are proportionally large, we provide a tight closed-form characterization of the test error and training loss achieved at the minima of the non-convex empirical loss. Using this high-dimensional characterization, we locate the positional-semantic phase transition, thus providing the first theoretical result about the emergence of sharp phase transitions in a model of dot-product attention.
- We contrast the performance of the dot-product attention layer with that of a linear attention layer, which can only implement positional mechanisms, and how the former outperforms the latter once it learns the semantic mechanism.

1.1 Related work

Theory of attention Attention models have been the object of sizeable theoretical scrutiny in recent years, with a growing body of work investigating various aspects such as their expressivity (Fu et al., 2023; Edelman et al., 2022; Hahn, 2020), inductive bias (Sahiner et al., 2022; Tarzanagh et al., 2023b,a), training dynamics (Jelassi et al., 2022; Boix-Adsera et al., 2023; Li et al., 2023a; Tian et al., 2023), and in-context learning (Bai et al., 2023; Guo et al., 2023; Li et al., 2023b; Zhang et al., 2023). Geshkovski et al. (2023) and Fu et al. (2023) analyze models with frozen non-trainable queries and keys, while Jelassi et al. (2022) similarly studies the learning of the value matrix and positional encodings only, fixing keys and queries to identity. The works of (Sahiner et al., 2022; Zhang et al., 2023) address trainable queries and keys for linear or ReLU-activated attention mechanisms. Li et al. (2023a); Edelman et al. (2022) provide error bounds for non-linear models, with trainable queries and keys. Because these studies are not tight, they do not allow to capture sharp changes in the behaviour of attention mechanisms such as phase transitions. A first tight analysis was provided in (Rende et al., 2023), in the context of learning a high-dimensional graphical model with factored attention, leveraging its formal equivalence to a linear and convex learning problem. The present manuscript conducts a tight analysis of the non-convex learning of a non-linear attention model with trainable tied queries and keys, thereby allowing the description of sharp phase transitions in the behaviour and performance of the model.

Positional encodings To combine the positional and semantic information in textual or general sequential data, a plethora of models and input encodings have been explored. Many approaches are based on autoregressive models, e.g. recurrent architectures (Elman, 1990), where the positional information is provided implicitly by the order in which the input is processed. While some transformers can leverage implicit positional information through causal masks in training (Haviv et al., 2022; Sinha et al., 2022; Kazemnejad et al., 2023), in principle a dot product attention layer requires an explicit encoding of positional information as it views the input sequence in parallel, as a bag of words (Vaswani et al., 2017). Several works experimentally explore different types of positional encodings with the goal of improving the downstream task performance (Shaw et al., 2018; Ruoss et al., 2023). In this work, we provide a tractable model to quantify the generalization error of a single layer of attention in the presence of positional encodings.

Mechanistic interpretability Recently, there has been an effort to reverse engineer the algorithms learned by a neural network for a specific task (Weiss et al., 2021; Olsson et al., 2022; Von Oswald et al., 2023) to uncover their limitations and generalization abilities. It has been shown that a transformer may implement two qualitatively different algorithms for modular addition (Zhong et al., 2023). In a similar spirit, our work provides examples of two tasks for which an attention layer can implement two qualitatively different solutions, based on either the positions or semantics of the inputs. While many works in mechanistic interpretability rely on a careful introspection and interpretation of the learned model to come to that conclusion, our second example allows for a theoretical analysis.

2 Two Solutions for the Histogram Task

In this section, we demonstrate that for a simple counting task two qualitatively different solutions exist in the loss landscape of a simple transformer using a dot-product attention layer with positional encodings. One solution corresponds to a dot-product attention matrix which is largely independent of the tokens making up the input sequence, and another strongly varies based on the tokens (and thus the semantic content of the input). Both solutions achieve a close to 100% test accuracy.

The training task is a sequence-to-sequence counting task, referred to as the *histogram task* in (Weiss et al., 2021). Given an input sequence $\mathbf{x} = [x_1, x_2, \dots, x_L]$ of length L of tokens from a fixed alphabet, the goal is to return a sequence $\mathbf{y} = [y_1, y_2, \dots, y_L]$, where each token y_i is the number of occurrences of the token x_i in \mathbf{x} . In Fig. 1 (A), we show an example where we consider sequences where the tokens are from the fixed alphabet $\mathcal{X} = \{A, B, C, \dots\}$ of size $|\mathcal{X}| = 15$. In this setting, for instance, the sequence $\mathbf{x} = [A, B, B, C, A, B]$ should be mapped to its histogram sequence $\mathbf{y} = [2, 3, 3, 1, 2, 3]$. When the input data is limited to length L , the output elements y_i thus take values up to the maximum count L .

We encode the input using token embeddings and absolute positional encodings which are trained jointly with the model weights. As an architecture we consider a small transformer made up of a single layer of dot-product attention, followed by a fully connected hidden layer and with learned embeddings for both tokens and positions. For each output position, it generates logits for the L possible classes of the output alphabet; training is done using the cross-entropy loss. Further details are provided in Appendix A.

We conduct experiments where we set two different sections of the models' weights to zero at the initialization of training –removing either the model's access to positional or semantic information, see Appendix A– and keeping the weights frozen throughout training with the Adam optimizer. After convergence, we check that the resulting

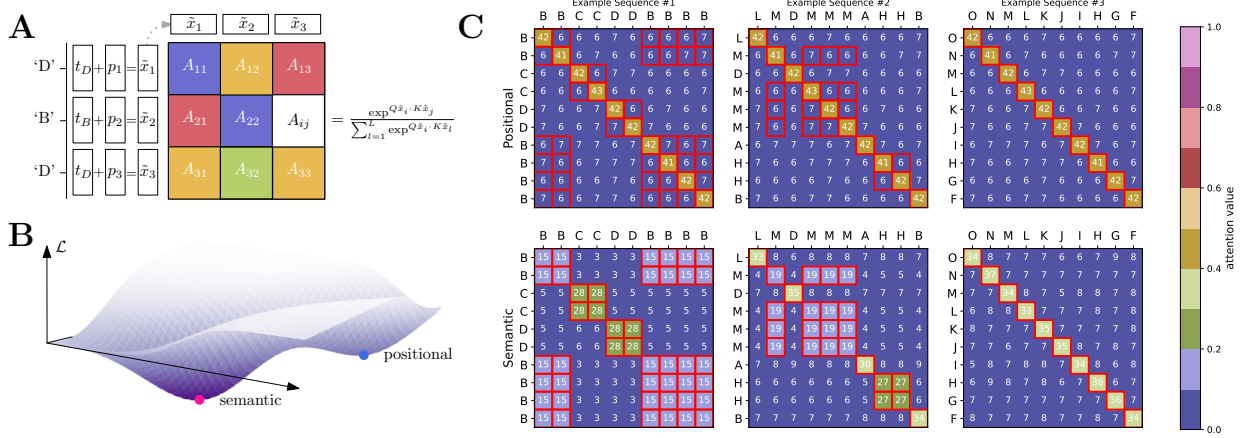


Figure 1: **Several solutions exist for the histogram task.** (A) The sequence $[D, B, D]$ is processed by a single layer of dot-product attention. After embedding each token into learned vectors $[t_D, t_B, t_D] \in \mathbb{R}^{3 \times d}$, the absolute positional encodings $[p_1, p_2, p_3]$ are added to give the inputs to the attention layer. The colored elements A_{ij} represent the values of the attention matrix, as generated using the key and query matrices Q and K and after applying softmax. (B) A schematic loss landscape containing two stable solutions. (C) Elements of attention matrices for the histogram task for local minima in the loss landscape. We generated a dataset of sequences by sampling each token of the sequence i.i.d. from the uniform distribution over all tokens. Models were trained with their respective frozen initialization using $n = 35,000$ samples and the Adam optimizer. *Top Row:* The attention matrix of the positional solution is largely independent of the specific input sequence. *Bottom Row:* The attention matrices from the semantic solution vary based on the input token. Red squares highlight the elements of A_{ij} where $x_i = x_j$.

configurations of weights are stable in the unconstrained loss landscape, i.e. without frozen weights. More precisely, we ascertain that these weights only change marginally when further trained with SGD on the unconstrained loss, and that the qualitative behaviour of the attention layer is retained. Our experiments demonstrate that the loss landscape of the transformer has at least two qualitatively different local minimizers (or close to minimizers), subsequently referred to as the semantic and positional solution.

We inspect the learnt attention matrix for different input sequences in Fig. 1 (C). The positional solution corresponds to a learnt attention matrix whose i, j -th component only depend on the positions i, j , and little on the tokens occupying these positions. The attention matrix is thus almost independent of the input sequence. In fact, the attention matrix is similar to the identity. In this case, the attention layer simply serves to aggregate the other tokens uniformly, and the fully connected layer learns the counting.

In contrast, the attention matrix learnt at the semantic solution displays larger i, j -th component if the tokens at position i and j are identical. In other words, identical tokens attend more to each other. This mechanism hence does not rely on the positions, but rather on the semantic content of the tokens. Both solutions and associated attention matrices thus correspond to feasible algorithms which ultimately allow the transformer to solve the downstream task.

Our experimental exploration gives compelling evidence that different stable solutions exist in the empirical loss landscape of simple transformers, which correspond to different algorithmic solutions to a given task. However, it remains an interpretation of an experiment and does not allow for a precise characterization of their behaviour or of the conditions under which they are established. In the remainder of this work, we turn to a simpler model of the attention layer, which presents similar phenomenology yet can be analyzed theoretically. More precisely, in Section 3, we provide a tight characterization of the global minimum of the empirical loss, and show in Section 5 that it corresponds to a semantic or positional mechanism, depending on the amount of training data and the task with a phase transition between them.

3 Tied low-rank attention model

This section introduces a simple model of supervised learning with an attention layer parametrized by learnable, tied and low-rank query and key matrices.

Input data model We consider a model of embedded sentences with uncorrelated (1-gram) words. More precisely, a sentence $x \in \mathbb{R}^{L \times d}$, where L is the sentence length and d represents the embedding dimension, consists of L tokens

$\{\mathbf{x}_\ell\}_{1 \leq \ell \leq L}$ independently drawn from a Gaussian distribution $\mathbf{x}_\ell \sim \mathcal{N}(0, \Sigma_\ell)$ with covariance $\Sigma_\ell \in \mathbb{R}^{d \times d}$. In the following, we denote the probability distribution of \mathbf{x} as p_x . Note that while this sentence model does not involve in itself statistical correlations between tokens, the task (target function) will entail interactions between different tokens.

Target function The target (teacher) is assumed to be of the form

$$y(x) = \mathsf{T} \left[\frac{1}{\sqrt{d}} \mathbf{x} \mathbf{Q}_* \right] \mathbf{x} \quad (1)$$

for $\mathsf{T} : \mathbb{R}^{L \times t} \rightarrow \mathbb{R}^{L \times L}$, and $\mathbf{x}_\ell \in \mathbb{R}^d$ is the ℓ -th word, i.e. the ℓ -th row of the sentence $\mathbf{x} \in \mathbb{R}^{L \times d}$. The term $\mathsf{T} \left[\frac{1}{\sqrt{d}} \mathbf{x} \mathbf{Q}_* \right] \in \mathbb{R}^{L \times L}$ in (1) should be interpreted as the target attention matrix, which mixes the tokens of the input \mathbf{x} , with and is parametrized by the matrix $\mathbf{Q}_* \in \mathbb{R}^{d \times r_t}$,

Tied attention We consider the learning of the target (1) using a parametric family of attention matrices

$$f_Q(x) = \mathsf{S} \left[\frac{1}{\sqrt{d}} (\mathbf{x} + \mathbf{p}) \mathbf{Q} \right] (\mathbf{x} + \mathbf{p}). \quad (2)$$

In (2), $\mathbf{p} \in \mathbb{R}^{L \times d}$ is a *fixed* matrix, corresponding to positional encodings, and $\mathbf{Q} \in \mathbb{R}^{d \times r_s}$ is a trainable matrix. We denote subsequently $\mathbf{p}_\ell \in \mathbb{R}^d$ the ℓ -th row of \mathbf{p} . Like the target (1), the parametric function (2) takes the form of a data-dependent attention matrix $\mathsf{S} \left[\frac{1}{\sqrt{d}} (\mathbf{x} + \mathbf{p}) \mathbf{Q} \right] \in \mathbb{R}^{L \times L}$ mixing the tokens of the input \mathbf{x} . Note that, compared to the usual attention mechanism (Vaswani et al., 2017), (2) corresponds to setting the value matrix to identity, and – since (2) is parametrized by a single matrix \mathbf{Q} – tying the key and query matrices.

Empirical risk minimization We study the learning of the attention layer (2), when a training set is $\mathcal{D} = \{\mathbf{x}^\mu, y(\mathbf{x}^\mu)\}_{\mu=1}^n$ with n independently sampled sentences $\{\mathbf{x}^\mu\}_{\mu=1}^n$ is available. The target (1) can be learnt by carrying out an empirical risk minimization:

$$\hat{\mathbf{Q}} = \underset{\mathbf{Q} \in \mathbb{R}^{d \times r}}{\operatorname{argmin}} \left[\sum_{\mu=1}^n \frac{1}{2d} \|y(\mathbf{x}^\mu) - f_Q(\mathbf{x}^\mu)\|^2 + \frac{\lambda}{2} \|\mathbf{Q}\|^2 \right]. \quad (3)$$

The performance of the resulting trained model $f_{\hat{\mathbf{Q}}}$ is measured at test time by the mean squared error (MSE)

$$\epsilon_g \equiv \frac{1}{dL} \mathbb{E}_{\mathbf{x} \sim p_x} \left\| y(\mathbf{x}) - f_{\hat{\mathbf{Q}}}(\mathbf{x}) \right\|^2. \quad (4)$$

4 Closed-form characterization of the training

High-dimensional limit We analyze the learning problem (3) in the limit where the embedding dimension d and the number of training samples n jointly tend to infinity, while their ratio $\alpha = n/d$ (henceforth referred to as the sample complexity) stays of order $\Theta_d(1)$. We further assume the sentence length L , the ranks r_s, r_t of the weights \mathbf{Q}, \mathbf{Q}_* , and the norm of the positional embeddings $\|\mathbf{p}\|$, to be $\Theta_d(1)$. We consider this limit as it permits a closed-form characterization presented in the next section. At the same time, this asymptotic limit exhibits rich learning phenomenology closely related to the experimental observations reported in Section 2, and which we further explore in Section (5).

The main technical result of the present work is a closed-form characterization of the test MSE (4) and training loss (3) achieved in the high-dimensional limit when training the model (2) via the empirical risk minimization of (3).

Assumption 4.1. *The covariances $\{\Sigma_\ell\}_{\ell=1}^L$ admit a common set of eigenvectors $\{\mathbf{e}_i\}_{i=1}^d$. We further note $\{\lambda_i^\ell\}_{i=1}^d$ the eigenvalues of Σ_ℓ . The eigenvalues $\{\lambda_i^\ell\}_{i=1}^d$ and the projection of the positional embedding \mathbf{p}_ℓ and the teacher rows \mathbf{Q}_j^* on the eigenvectors $\{\mathbf{e}_i^\top \mathbf{p}_\ell\}_{i,\ell}, \{\mathbf{e}_i^\top \mathbf{Q}_j^*\}_{i,j}$ are assumed to admit a well-defined joint distribution ν as $d \rightarrow \infty$ – namely, for $\gamma = (\gamma_1, \dots, \gamma_L) \in \mathbb{R}^L, \pi = (\pi_1, \dots, \pi_t) \in \mathbb{R}^t$ and $\tau = (\tau_1, \dots, \tau_L) \in \mathbb{R}^L$:*

$$\frac{1}{d} \sum_{i=1}^d \prod_{k=1}^K \prod_{j=1}^t \delta \left(\lambda_i^\ell - \gamma_\ell \right) \delta \left(\sqrt{d} \mathbf{e}_i^\top \mathbf{p}_\ell - \tau_\ell \right) \delta \left(\mathbf{e}_i^\top \mathbf{Q}_j^* - \pi_j \right) \xrightarrow{d \rightarrow \infty} \nu(\gamma, \tau). \quad (5)$$

Moreover, the marginals ν_γ (resp. ν_τ) are assumed to have a well-defined first (resp. second) moment.

Result 4.2. Under Assumption 4.1, in the limit $n, d \rightarrow \infty, \|\mathbf{p}_\ell\|, n/d, L, r_s, r_t = \Theta_d(1)$, the summary statistics

$$\begin{aligned} \rho_\ell &\equiv \frac{\mathbf{Q}_*^\top \Sigma_\ell \mathbf{Q}_*}{d} \in \mathbb{R}^{r_t \times r_t}, & q_\ell &\equiv \frac{\hat{\mathbf{Q}}^\top \Sigma_\ell \hat{\mathbf{Q}}}{d} \in \mathbb{R}^{r_s \times r_s}, \\ m_\ell &\equiv \frac{\hat{\mathbf{Q}}^\top \mathbf{p}_\ell}{d} \in \mathbb{R}^{r_s}, & \theta_\ell &\equiv \frac{\hat{\mathbf{Q}}^\top \Sigma_\ell \mathbf{Q}_*}{d} \in \mathbb{R}^{r_s \times r_t} \end{aligned} \quad (6)$$

concentrate in probability, and are solutions of the set of finite-dimensional self-consistent equations

$$\left\{ \begin{array}{l} q_\ell = \int d\nu(\gamma, \tau, \pi) \gamma_\ell \left(\lambda \mathbb{I}_r + \sum_{\kappa=1}^L \gamma_\kappa \hat{V}_\kappa \right)^{-2} \\ \quad \left(\sum_{\kappa=1}^L \gamma_\kappa \hat{q}_\kappa + \left(\sum_{\kappa=1}^L \hat{m}_\kappa \tau_\kappa + \gamma_\kappa \hat{\theta}_\kappa \cdot \pi \right)^{\otimes 2} \right) \\ V_\ell = \int d\nu(\gamma, \tau, \pi) \gamma_\ell \left(\lambda \mathbb{I}_r + \sum_{\kappa=1}^L \gamma_\kappa \hat{V}_\kappa \right)^{-1} \\ m_\ell = \int d\nu(\gamma, \tau, \pi) \tau_\ell \left(\lambda \mathbb{I}_r + \sum_{\kappa=1}^L \gamma_\kappa \hat{V}_\kappa \right)^{-1} \\ \quad \left(\sum_{\kappa=1}^L \hat{m}_\kappa \tau_\kappa + \gamma_\kappa \hat{\theta}_\kappa \cdot \pi \right) \\ \theta_\ell = \int d\nu(\gamma, \tau, \pi) \gamma_\ell \left(\lambda \mathbb{I}_r + \sum_{\kappa=1}^L \gamma_\kappa \hat{V}_\kappa \right)^{-1} \\ \quad \left(\sum_{\kappa=1}^L \hat{m}_\kappa \tau_\kappa + \gamma_\kappa \hat{\theta}_\kappa \cdot \pi \right) \pi^\top. \end{array} \right. , \quad \left\{ \begin{array}{l} \hat{q}_\ell = \alpha \mathbb{E}_{\Xi, U} V_\ell^{-1} \left(\text{prox}(\Xi, U)_\ell - q_\ell^{\frac{1}{2}} \xi_\ell - m_\ell \right)^{\otimes 2} V_\ell^{-1} \\ \hat{V}_\ell = q_\ell^{-1} \hat{\theta}_\ell \theta_\ell^\top - \alpha q_\ell^{-\frac{1}{2}} \mathbb{E}_{\Xi, U} V_\ell^{-1} \left(\text{prox}(\Xi, U)_\ell - q_\ell^{\frac{1}{2}} \xi_\ell - m_\ell \right) \xi_\ell^\top \\ \hat{m}_\ell = \alpha \mathbb{E}_{\Xi, U} V_\ell^{-1} \left(\text{prox}(\Xi, U)_\ell - q_\ell^{\frac{1}{2}} \xi_\ell - m_\ell \right) \\ \hat{\theta}_\ell = \alpha \mathbb{E}_{\Xi, U} V_\ell^{-1} \left(\text{prox}(\Xi, U)_\ell - q_\ell^{\frac{1}{2}} \xi_\ell - m_\ell \right) \\ \quad \left(u_\ell - \xi_\ell^\top q_\ell^{-1/2} \theta_\ell \right)^\top \left(\rho_\ell - \theta_\ell^\top q_\ell^{-1} \theta_\ell \right)^{-1} \end{array} \right. \quad (7)$$

In (7), $U = \{u_\ell\}_{\ell=1}^L$ and $\Xi = \{\xi_\ell\}_{\ell=1}^L$, with $u_\ell \sim \mathcal{N}(\xi_\ell^\top q_\ell^{-1/2} \theta_\ell, \rho_\ell - \theta_\ell^\top q_\ell^{-1} \theta_\ell)$ and $\xi_\ell \sim \mathcal{N}(0, \mathbb{I}_r)$, and $\cdot^{\otimes 2}$ denotes the outer product of a vector with itself. Finally, the resolvents $\{\text{prox}(\Xi, U)_\ell\}_{\ell=1}^L$ are defined as the minimizers of the Moreau envelope

$$\mathcal{M}(\Xi, U) = \inf_{z_1, \dots, z_L} \frac{1}{2} \left\{ \sum_{\ell=1}^L \text{Tr} \left[V_\ell^{-1} \left(x_\ell - q_\ell^{1/2} \xi_\ell - m_\ell \right)^{\otimes 2} \right] + \text{Tr} \left[\mathbf{S}(Z) \rho_\Sigma \mathbf{S}(Z)^\top \right] - 2 \text{Tr} \left[\mathbf{T}(U) \rho_\Sigma \mathbf{S}(Z)^\top \right] \right\}. \quad (8)$$

We noted $Z \in \mathbb{R}^{L \times r_s}$ (resp. $U \in \mathbb{R}^{L \times r_t}$) the matrix whose rows are z_ℓ (resp. u_ℓ). In (8),

$$\rho_\Sigma \equiv \text{diag} \left[\left(\int d\nu(\gamma, \tau) \gamma_\ell \right)_{\ell=1}^L \right] \in \mathbb{R}^{L \times L}. \quad (9)$$

In the same limit, the test error (4) converges in probability to

$$\epsilon_g = \mathbb{E}_h \text{Tr} \left[\mathbf{S}[h] \rho_\Sigma \mathbf{S}[h]^\top \right] + \mathbb{E}_{h^*} \text{Tr} \left[\mathbf{T}[h^*] \rho_\Sigma \mathbf{T}[h^*]^\top \right] - 2 \mathbb{E}_{h, h^*} \text{Tr} \left[\mathbf{S}[h] \rho_\Sigma \mathbf{T}[h^*]^\top \right]. \quad (10)$$

where the average bears on $h \in \mathbb{R}^{L \times r_s}$, $h^* \in \mathbb{R}^{L \times r_t}$ with independent rows with statistics

$$(h_\ell, h_\ell^*) \sim \mathcal{N} \left[\begin{pmatrix} m_\ell \\ 0 \end{pmatrix}, \begin{pmatrix} q_\ell & \theta_\ell \\ \theta_\ell^\top & \rho_\ell \end{pmatrix} \right] \quad (11)$$

Finally, the training loss ϵ_t converges in probability to

$$\epsilon_t = \alpha \mathbb{E}_{Y, \Xi} \mathcal{M} - \frac{1}{2} \sum_{\ell=1}^L \text{Tr} [\hat{q}_\ell V_\ell] + \frac{\lambda}{2} \int d\nu(\gamma, \tau) \text{Tr} \left[\left(\lambda + \sum_{\ell=1}^L \gamma_\ell \hat{V}_\ell \right)^{-1} \left(\sum_{\ell=1}^L \gamma_\ell \hat{q}_\ell + \left(\sum_{\ell=1}^L \tau_\ell \hat{m}_\ell + \hat{\theta}_\ell \cdot \pi \right)^{\otimes 2} \right) \right]. \quad (12)$$

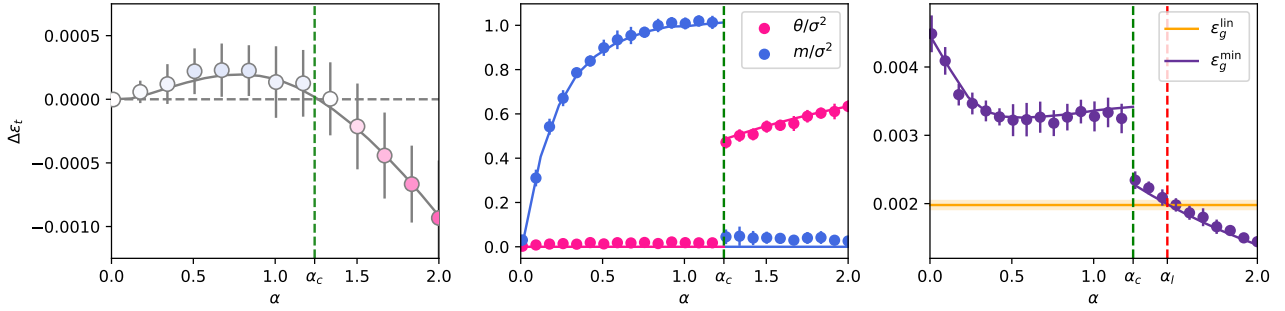


Figure 2: Mixed positional/semantic teacher for $\omega = 0.3$. Setting is $r_s = r_t = 1$, $L = 2$, $A = ((0.6, 0.4), (0.4, 0.6))$, $\Sigma_1 = \Sigma_2 = 0.25\mathbb{I}_d$, $\mathbf{p}_1 = \mathbf{1}_d = -\mathbf{p}_2$ and $\mathbf{Q}_* \sim \mathcal{N}(0, \mathbb{I}_d)$. **(left)** Solid lines: difference in training loss $\Delta\epsilon_t$ between the semantic and positional solutions of (7) in Result 4.2. Markers: difference in training loss at convergence achieved by training the model (2) using gradient descent initialized resp. at \mathbf{Q}_* and at \mathbf{p}_1 . Marker color according to phase diagram in Fig. 3. **(middle)** (blue) overlap θ between the learnt weights $\hat{\mathbf{Q}}$ and the target weights \mathbf{Q}_* (red) overlap m between the learnt weights $\hat{\mathbf{Q}}$ and the positional embedding \mathbf{p}_1 . Solid lines represent the theoretical characterization of these two summary statistics provided by Result 4.2. Only the solution of (7) corresponding to the lowest found training loss is represented (respectively the positional solution for $\alpha < \alpha_c$ and the semantic solution for $\alpha > \alpha_c$). Markers represent experimental measures of these quantities, for gradient descent at convergence. Gradient descent was initialized at \mathbf{p}_1 for $\alpha < \alpha_c$ and at \mathbf{Q}_* for $\alpha > \alpha_c$. **(right)** Test MSE. Solid lines represent the theoretical characterization of Result 4.2. Only the solution corresponding to minimal training loss is represented. Markers indicate the MSE experimentally reached by the model (2) trained using gradient descent, initialized at \mathbf{p}_1 for $\alpha < \alpha_c$ and at \mathbf{Q}_* for $\alpha > \alpha_c$. The yellow line represents the MSE achieved by the dense linear baseline (15), as analytically characterized by Result 5.1. All experiments were performed in $d = 1,000$ with the pytorch implementation of full-batch gradient descent, for $T = 5,000$ epochs and learning rate $\eta = 0.15$. All points are averaged over 24 instances of the problem each.

The derivation of Result 4.2 is provided in Appendices (B), and is exploiting a mapping of the model (2) to a (variant of) a Generalized Linear Model (GLM) (Nelder & Wedderburn, 1972; McCullagh, 1919). The summary statistics characterized by the equations (7) (often called state evolution (Javanmard & Montanari, 2013) in this context) asymptotically describe the fixed points of a Generalized Approximate Message Passing (GAMP) algorithm (Rangan et al., 2016), which we state in Appendix B. The stable fixed points of GAMP in turn correspond to critical (zero-gradient) points of the non-convex empirical loss landscape (3). Therefore, while Result (4.2) is stated as a characterization of the global minimum of (3), which is the main concern of the present work, solutions of (7) also describe local minima.

This strategy to study asymptotics of high-dimensional problem has been used in many recent work, see e.g. (Bayati & Montanari, 2011b; Donoho & Montanari, 2016; Emami et al., 2020; Loureiro et al., 2021; Gerbelot et al., 2022). We note, however, that we importantly assume the point-wise convergence of GAMP. While we believe that this point can be rigorously justified, it would require a considerable amount of work—in particular, the usual rigorous tools used in recent works fall short because of the non-convexity of the loss—and we leave this point for further studies (see the discussion in App. C, where we also provide an alternative derivation using the replica method from statistical physics (Parisi, 1979)). Finally, we mention that while Result 4.2 is presented for an ℓ_2 regularization of the empirical loss (3) for clarity, similar results can be reached for generic convex regularizers, and are presented in Appendix C. In the following section, we explore the phenomenology uncovered from the study of the equations (7) of Result 4.2, for the special case of dot-product attention.

5 Positional-to-semantic phase transition

5.1 Rank one dot-product attention

In the following, we turn to a special case of tied low-rank attention (2), which exhibits a similar phenomenology as the histogram task empirically probed in Section 2 – namely a dot-product attention layer:

$$\mathbf{S} \left[\frac{1}{\sqrt{d}}(\mathbf{x} + \mathbf{p})\mathbf{Q} \right] = \text{softmax} \left(\frac{1}{d}(\mathbf{x} + \mathbf{p})\mathbf{Q}\mathbf{Q}^\top(\mathbf{x} + \mathbf{p})^\top \right). \quad (13)$$

As in (2), we allow for positional encodings \mathbf{p} in the dot-product attention parametrization (13). We further consider a specific case of target attention matrix (1) of the form

$$\mathbb{T} \left[\frac{1}{\sqrt{d}} \mathbf{x} \mathbf{Q}_* \right] = (1 - \omega) \text{softmax} \left(\frac{1}{d} \mathbf{x} \mathbf{Q}_* \mathbf{Q}_*^\top \mathbf{x}^\top \right) + \omega A. \quad (14)$$

with $A \in \mathbb{R}^{L \times L}$ a fixed matrix. In (14), the parameter $\omega \in [0, 1]$ tunes the relative strength of the dot-product term and the fixed matrix term, and interpolates between a fully positional and a fully semantic task:

- For $\omega = 0$, the target reduces to the first dot-product term, and is purely semantic, in that the i, j -th element of the score matrix $\text{softmax}(\frac{1}{d} \mathbf{x} \mathbf{Q}_* \mathbf{Q}_*^\top \mathbf{x}^\top)$ only depends on the tokens $\mathbf{x}_i, \mathbf{x}_j$ and not explicitly on their respective placements i, j inside the sentence. To learn satisfyingly the target, the learning model thus has to learn a *semantic* attention matrix.
- For $\omega = 1$, the target reduces to the second fixed term A in (14). The attention matrix A associated thereto is purely positional, in the sense that A_{ij} is a function of i, j but not of $\mathbf{x}_i, \mathbf{x}_j$. To complete the learning task, a *positional* mechanism thus needs to be learnt.

The parameter ω thus allows to tune the extent to which the task requires the model to implement semantic attention (small ω s) or rather positional attention (large ω s).

In the following, for definiteness, we further assume $r_s = r_t = 1$ and set \mathbf{Q}_* to be a fixed random Gaussian vector drawn from $\mathcal{N}(0, \mathbb{I}_d)$, and choose the positional encodings $\mathbf{p}_1 = -\mathbf{p}_2 = \mathbf{1}_d$. Finally, for simplicity, we consider sentences with two tokens $L = 2$ and isotropic token covariances $\Sigma_1 = \Sigma_2 = \sigma^2 \mathbb{I}_d$.

5.2 Semantic and positional mechanisms

The summary statistics θ_ℓ, m_ℓ describing the global minimizer of the empirical loss minimization (3) of the dot-product attention (13) on the target (14) are captured alongside the corresponding test error (4) and training loss (3), by Result 4.2. The solution of the system of equations (7) is not unique, and different stable fixed points describe different corresponding critical points of the non-convex empirical loss landscape (3). In practice, we notably find two solutions of (7), corresponding to two different mechanisms implemented by the dot-product attention (13) when approximating the target (14):

- *Positional solution*– One solution of (7) correspond to vanishing overlap $\theta = 0$ between the trained weights $\hat{\mathbf{Q}}$ and the semantic target weights \mathbf{Q}_* , and non-zero $m > 0$ between the trained weights $\hat{\mathbf{Q}}$ and the positional embedding $\mathbf{p}_1 = -\mathbf{p}_2$. Consequently, the argument of the dot-product attention $\hat{\mathbf{Q}}(\mathbf{x} + \mathbf{p})$ has a sizeable token-independent –thus positional– contribution $\hat{\mathbf{Q}}\mathbf{p}$, alongside a token-dependent semantic part $\hat{\mathbf{Q}}\mathbf{x}$. Because of the positional term, the elements of the resulting learnt attention matrix $\text{softmax}(\frac{1}{d}(\mathbf{x} + \mathbf{p})\hat{\mathbf{Q}}\hat{\mathbf{Q}}^\top(\mathbf{x} + \mathbf{p})^\top)$ implement a partly positional mechanism.
- *Semantic solution*– Another solution of the system of equations (7) is associated to vanishing overlap $m = 0$ between the learnt weights $\hat{\mathbf{Q}}$ and the positional embeddings, and finite overlap $\theta > 0$ with the target weights \mathbf{Q}_* . Therefore the resulting learnt attention matrix $\text{softmax}(\frac{1}{d}(\mathbf{x} + \mathbf{p})\hat{\mathbf{Q}}\hat{\mathbf{Q}}^\top(\mathbf{x} + \mathbf{p})^\top) \approx \text{softmax}(\frac{1}{d}\mathbf{x}\hat{\mathbf{Q}}\hat{\mathbf{Q}}^\top\mathbf{x}^\top)$ is largely semantic.

While the system of self-consistent equations (7) may admit other solutions, we did not find solutions with lower training loss than the two aforescribed fixed points. Which of these solution corresponds to the global minimum – and thus the solution of the optimization (3)– depends on the sample complexity α and the positional/semantic parameter ω (14), as we describe in the following subsection.

5.3 Positional-to-semantic phase transition

For a fixed parameter ω in (14), an analysis of equations (7), further detailed in Appendix C, reveals that for a sizeable range of ω , in the probed setups, there exists a threshold α_c for the sample complexity so that

- For $\alpha < \alpha_c$, the global minimum of (3) corresponds to a positional mechanism, and is described by the positional solution of (7) of Result 4.2 with $\theta = 0, m > 0$.
- For $\alpha > \alpha_c$, the global minimum of (3) corresponds to a semantic mechanism, and is described by the semantic solution of (7) of Result 4.2 with $\theta > 0, m = 0$.

The dot-product attention thus displays a phase transition in sample complexity from a positional mechanism to a semantic mechanism, implementing the simpler positional mechanism when having access to small amounts of data, and only learning the semantic content of the target (14) when presented sufficient data. The critical sample complexity α_c generically grows with the positionality ω of the target function (14), as the semantic content – i.e. the first term of (14) – is less apparent for larger ω , and thus require larger amounts of data to be identified and approximated by the dot-product attention (13). An example for $\omega = 0.3$ is given in Fig. 2.

Algorithmically, the positional minimum can be reached for $\alpha < \alpha_c$ by gradient descent by initializing the weights \mathbf{Q} of the attention (13) close to the positional embedding \mathbf{p}_1 . By the same token, the semantic minimum can be reached by gradient descent from an initialization at the teacher weights \mathbf{Q}_* (14). Henceforth, we refer with a slight abuse to the minimum experimentally reached from a positional (resp. semantic) initialization as the positional (resp. semantic) minimum, even when it is not global. Finally, note importantly that the semantic initialization is informed by nature, in that it necessitates the knowledge of the target parameters \mathbf{Q}_* . A precise analysis of the dynamics of gradient descent from an agnostic (random) initialization, and ascertaining whether the optimizer reaches the global minimum, is an interesting question which falls out of the scope of the present manuscript – whose aim is rather to provide a characterization of the global minimum alone.

The difference in training loss $\Delta\epsilon_t$ between the positional and semantic solutions of (7) is represented in Fig. 3, alongside the difference in training loss at convergence experimentally reached by gradient descent from a positional ($\mathbf{Q} = \mathbf{p}_1$) and semantic ($\mathbf{Q} = \mathbf{Q}_*$) initializations. For small (resp. large) sample complexity $\alpha < \alpha_c$ (resp. $\alpha > \alpha_c$), the training loss of the positional (resp. semantic) minimum is lower, and thus corresponds to the global minimum.

The analytical equations (7) are observed to capture well the difference in training loss between both minima (global and local) across the whole range of probed sample complexities, see Fig. 2. Finally, Fig. 2 (middle, right) presents the theoretical predictions of Result 4.2 for the weights/target and weights/embedding overlaps θ , m and the generalization MSE ϵ_g achieved at the global minimum of the loss landscape (3). These analytical characterizations are compared with experimental estimates of the same metrics obtained by optimizing (3) with the Pytorch (Paszke et al., 2019) implementation of gradient descent, from a positional (resp. semantic) initialization for $\alpha < \alpha_c$ (resp. $\alpha > \alpha_c$), displaying overall good agreement. In Appendix E.1 we verify that in the scaling limit of our analysis, namely $n, d \rightarrow \infty$ for $\alpha = O(1)$, the agreement improves. We explore a random initialization of \mathbf{Q} in Appendix E.3, showing that it may reach either of the local minima, or get stuck in a different one.

The dot-product attention (13) thus implements a semantic mechanism when learning from sufficient amounts of data. The learning of the semantic mechanism by the dot-product attention at sample complexities $\alpha > \alpha_c$ corresponds to a noticeable drop in the generalization MSE as can be observed in Fig. 2, right. But just how essential is the learning of semantic mechanism in the ability of the dot-product attention to generalize well? We explore this question in the following subsection, by comparing the dot-product attention (13) to a purely positional attention model.

5.4 Purely positional baseline

In this subsection, for the same target (14), we contrast the dot-product attention model (13), analyzed in the previous subsections, to the baseline given by a linear attention layer:

$$f_W(\mathbf{x}) = W \cdot \mathbf{x}, \quad (15)$$

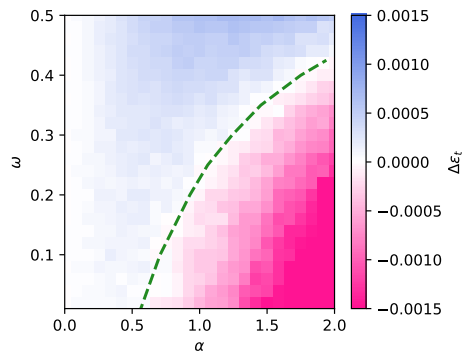


Figure 3: Phase transition between semantic and positional training loss. and $r_s = r_t = 1, L = 2, A = ((0.6, 0.4), (0.4, 0.6)), \Sigma_1 = \Sigma_2 = 0.25\mathbb{I}_d, \mathbf{p}_1 = \mathbf{1} = -\mathbf{p}_2$ and $\mathbf{Q}_* \sim \mathcal{N}(0, \mathbb{I}_d)$. The color map represents the difference in training loss at convergence when training the model (2) using the Pytorch implementation of full-batch gradient descent, respectively from an initialization at \mathbf{p}_1 and an initialization at \mathbf{Q}_* . The green dashed lines represents the theoretical prediction for the threshold $\alpha_c(\omega)$ above which the semantic solution of (7) in Result 4.2 has lower loss than the positional solution. Experiments were performed as in Fig. 2.

with a trainable weights matrix $W \in \mathbb{R}^{L \times L}$. As for the dot-product attention (13), we consider the case where the weights \hat{W} are learnt by minimizing the empirical risk

$$\hat{W} = \operatorname{argmin}_{W \in \mathbb{R}^{L \times L}} \sum_{\mu=1}^n \|y(\mathbf{x}^\mu) - f_W(\mathbf{x}^\mu)\|^2 \quad (16)$$

The model (15) is a natural counterpart to the dot-product architecture (13). In (15), the attention matrix is parametrized by a single fully-trainable matrix W , instead of being parametrized as a dot-product attention as in (13). A seminal difference in the two parametrizations is that while the elements of $\operatorname{softmax}(1/d \mathbf{x} \mathbf{Q} \mathbf{Q}^\top \mathbf{x}^\top)$ can depend on the input tokens \mathbf{x} , and therefore express semantic information, the elements W_{ij} of W can only depend on the positions i, j . The model (15) can thus only implement *positional mechanisms*, while the dot-product attention (13) can implement both linear and semantic mechanisms, as discussed above. Finally, observe that the model (15) is closely related to the one analyzed by (Rende et al., 2023) in another asymptotic limit. The following result characterizes the test error achieved by the purely positional model (15):

Result 5.1. *In the same asymptotic limit as Result (4.2), the learnt weights \hat{W} trained by minimizing the empirical risk (16) coincide with the minimizer of the population square risk, and thus admit the compact expression*

$$\hat{W} = \mathbb{E}_{\mathbf{x}} \mathbb{T} \left[\frac{1}{\sqrt{d}} \mathbf{x} \mathbf{Q}_* \right] = \mathbb{E}_h \mathbb{T}[h] \quad (17)$$

where the average bears over a finite-dimensional matrix $h \in \mathbb{R}^{L \times t}$ with independent rows h_ℓ with statistics $h_\ell \sim \mathcal{N}(0, \rho_\ell)$, where ρ_ℓ was defined in (6) in Result (4.2). We remind that $\mathbb{T} \left[\frac{1}{\sqrt{d}} \mathbf{x} \mathbf{Q}_* \right]$ corresponds to the target score matrix (1). Finally, the test MSE $1/dL \mathbb{E}_{\mathbf{x}} \|y(\mathbf{x}) - f_{\hat{W}}(\mathbf{x})\|^2$ achieved by the trained dense linear model $f_{\hat{W}}$ (15) admits the asymptotic characterization

$$\epsilon_g^{\text{lin}} = \frac{1}{L} \operatorname{Tr} \left[\hat{W} \rho_\Sigma \hat{W}^\top \right] + \frac{1}{L} \mathbb{E}_h \operatorname{Tr} \left[\mathbb{T}[h] \rho_\Sigma \mathbb{T}[h]^\top \right] - \frac{2}{L} \mathbb{E}_h \operatorname{Tr} \left[\hat{W} \rho_\Sigma \mathbb{T}[h]^\top \right]. \quad (18)$$

The MSE achieved by the baseline (15) when learning the target (14) is plotted in Fig. 2 (right) as the orange solid line, alongside the MSE achieved by the dot-product attention (13) discussed in previous subsections. Remarkably, in the setup of Fig. 2, in the positional regime $\alpha < \alpha_c$ when the dot-product attention relies on a positional mechanism $\theta = 0, m > 0$ to approximate the target, the dot-product attention (13) is outperformed by the purely positional attention (15) $\epsilon_g > \epsilon_g^{\text{lin}}$. In contrast, in the semantic regime $\alpha > \alpha_c$ where the dot-product attention learns the semantic mechanism, there exists a sample complexity $\alpha_l \geq \alpha_c$ above which $\epsilon_g < \epsilon_g^{\text{lin}}$, i.e. the dot-product attention (13) outperforms the dense linear baseline (15). This threshold value α_l is plotted for various positionality strengths ω in Fig. 4, alongside the positional-to-semantic threshold α_c . Interestingly, we observe $\alpha_l \geq \alpha_c$ in all probed settings, temptingly suggesting the natural interpretation that the dot-product attention needs to learn the semantic mechanism first (at $\alpha = \alpha_c$) in order to then be able to outperform the best positional approximation $f_{\hat{W}}$ (at $\alpha = \alpha_l$). This highlights the importance of the semantic mechanism, enabled by the dot-product parametrization (13), in learning targets with semantic content such as (14).

Conclusion

We explored the interplay between positional and semantic attention, both through an empirical example and the prism of tied low-rank self-attention in high dimensions. In the empirical setting we showed how a simple algorithmic counting

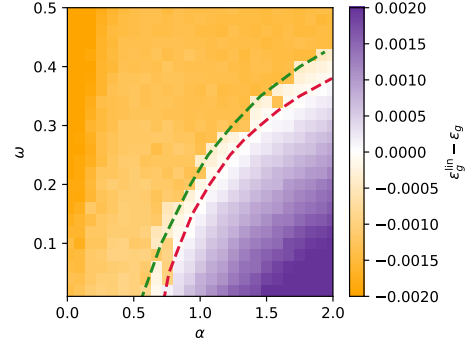


Figure 4: Phase transition between semantic and positional training loss. $r_s = r_t = 1, L = 2, A = ((0.6, 0.4), (0.4, 0.6)), \Sigma_1 = \Sigma_2 = 0.25 \mathbb{I}_d, \mathbf{p}_1 = \mathbf{1} = -\mathbf{p}_2$ and $\mathbf{Q}_* \sim \mathcal{N}(0, \mathbb{I}_d)$. The color map represents the difference in test MSE at convergence when training the model (13) using the Pytorch implementation of full-batch gradient descent initialized at \mathbf{Q}_* , and the dense linear baseline (15). The red dashed lines indicate the theoretical prediction –following from Result 4.2 and Result 15– for the threshold sample complexity α_l above which the dot-product attention (2) outperforms the baseline (15). For comparison, the positional-to-semantic threshold $\alpha_c(\omega)$ is reminded in green. Experiments were performed as in Fig. 2.

task can be solved using a positional or semantic mechanism in the attention layer. For a different task, in a theoretically controlled setting, we characterized the global optimum of the empirical loss, when learning a target attention layer. This global optimum was found to correspond to either a positional or a semantic mechanism, with a phase transition between the two mechanisms occurring as the sample complexity increases. We believe the present asymptotic analysis of the inner workings of attention mechanisms opens up exciting research directions. Considering untied query and key matrices, appending a readout network after the attention layer, or addressing more practical training procedures such as masked language modelling, are some possible extensions which will hopefully pave the way towards a satisfactory theoretical comprehension of attention mechanisms.

Acknowledgements

We thank Luca Biggio, Federica Gerace, and Matteo Vilucchio for insightful discussions. We acknowledge funding from the Swiss National Science Foundation grant SNFS OperaGOST (grant number 200390), and SMARtNet (grant number 212049).

References

- Aubin, B., Maillard, A., Krzakala, F., Macris, N., Zdeborová, L., et al. The committee machine: Computational to statistical gaps in learning a two-layers neural network. *Advances in Neural Information Processing Systems*, 31, 2018.
- Bai, Y., Chen, F., Wang, H., Xiong, C., and Mei, S. Transformers as statisticians: Provable in-context learning with in-context algorithm selection. *arXiv preprint arXiv:2306.04637*, 2023.
- Bayati, M. and Montanari, A. The dynamics of message passing on dense graphs, with applications to compressed sensing. *IEEE Transactions on Information Theory*, 57(2):764–785, 2011a.
- Bayati, M. and Montanari, A. The lasso risk for gaussian matrices. *IEEE Transactions on Information Theory*, 58(4):1997–2017, 2011b.
- Boix-Adsera, E., Littwin, E., Abbe, E., Bengio, S., and Susskind, J. Transformers learn through gradual rank increase. *arXiv preprint arXiv:2306.07042*, 2023.
- Bolthausen, E. An iterative construction of solutions of the tap equations for the sherrington–kirkpatrick model. *Communications in Mathematical Physics*, 325(1):333–366, 2014.
- Clarté, L., Loureiro, B., Krzakala, F., and Zdeborová, L. Theoretical characterization of uncertainty in high-dimensional linear classification. *Machine Learning: Science and Technology*, 4(2):025029, 2023.
- Cornacchia, E., Mignacco, F., Veiga, R., Gerbelot, C., Loureiro, B., and Zdeborová, L. Learning curves for the multi-class teacher–student perceptron. *Machine Learning: Science and Technology*, 4(1):015019, 2023.
- Cui, H. and Zdeborová, L. High-dimensional asymptotics of denoising autoencoders. *arXiv preprint arXiv:2305.11041*, 2023.
- Donoho, D. and Montanari, A. High dimensional robust m-estimation: Asymptotic variance via approximate message passing. *Probability Theory and Related Fields*, 166:935–969, 2016.
- d’Ascoli, S., Sagun, L., Biroli, G., and Bruna, J. Finding the needle in the haystack with convolutions: on the benefits of architectural bias. In Wallach, H., Larochelle, H., Beygelzimer, A., d’Alché-Buc, F., Fox, E., and Garnett, R. (eds.), *Advances in Neural Information Processing Systems*, volume 32. Curran Associates, Inc., 2019.
- Edelman, B. L., Goel, S., Kakade, S., and Zhang, C. Inductive biases and variable creation in self-attention mechanisms. In *International Conference on Machine Learning*, pp. 5793–5831. PMLR, 2022.
- Elman, J. L. Finding structure in time. *Cognitive Science*, 14(2):179–211, 1990. ISSN 0364-0213. doi: [https://doi.org/10.1016/0364-0213\(90\)90002-E](https://doi.org/10.1016/0364-0213(90)90002-E).
- Emami, M., Sahraee-Ardakan, M., Pandit, P., Rangan, S., and Fletcher, A. Generalization error of generalized linear models in high dimensions. In *International Conference on Machine Learning*, pp. 2892–2901. PMLR, 2020.

- Fu, H., Guo, T., Bai, Y., and Mei, S. What can a single attention layer learn? a study through the random features lens. *arXiv preprint arXiv:2307.11353*, 2023.
- Gerbelot, C., Abbara, A., and Krzakala, F. Asymptotic errors for teacher-student convex generalized linear models (or: How to prove kabashima’s replica formula). *IEEE Transactions on Information Theory*, 69(3):1824–1852, 2022.
- Geshkovski, B., Letrouit, C., Polyanskiy, Y., and Rigollet, P. A mathematical perspective on transformers. *arXiv preprint arXiv:2312.10794*, 2023.
- Gordon, Y. On milman’s inequality and random subspaces which escape through a mesh in \mathbb{R}^n . In *Geometric Aspects of Functional Analysis: Israel Seminar (GAFA) 1986–87*, pp. 84–106. Springer, 1988.
- Guo, T., Hu, W., Mei, S., Wang, H., Xiong, C., Savarese, S., and Bai, Y. How do transformers learn in-context beyond simple functions? a case study on learning with representations. *arXiv preprint arXiv:2310.10616*, 2023.
- Hahn, M. Theoretical limitations of self-attention in neural sequence models. *Transactions of the Association for Computational Linguistics*, 8:156–171, 2020.
- Haviv, A., Ram, O., Press, O., Izsak, P., and Levy, O. Transformer language models without positional encodings still learn positional information. In Goldberg, Y., Kozareva, Z., and Zhang, Y. (eds.), *Findings of the Association for Computational Linguistics: EMNLP 2022*, pp. 1382–1390, Abu Dhabi, United Arab Emirates, December 2022. Association for Computational Linguistics. doi: 10.18653/v1/2022.findings-emnlp.99.
- Javanmard, A. and Montanari, A. State evolution for general approximate message passing algorithms, with applications to spatial coupling. *Information and Inference: A Journal of the IMA*, 2(2):115–144, 2013.
- Jelassi, S., Sander, M., and Li, Y. Vision transformers provably learn spatial structure. *Advances in Neural Information Processing Systems*, 35:37822–37836, 2022.
- Kazemnejad, A., Padhi, I., Natesan, K., Das, P., and Reddy, S. The impact of positional encoding on length generalization in transformers. In *Thirty-seventh Conference on Neural Information Processing Systems*, 2023.
- Li, H., Wang, M., Liu, S., and Chen, P.-Y. A theoretical understanding of shallow vision transformers: Learning, generalization, and sample complexity. *arXiv preprint arXiv:2302.06015*, 2023a.
- Li, Y., Ildiz, M. E., Papailiopoulos, D., and Oymak, S. Transformers as algorithms: Generalization and stability in in-context learning. In *International Conference on Machine Learning*, pp. 19565–19594. PMLR, 2023b.
- Loureiro, B., Sicuro, G., Gerbelot, C., Pacco, A., Krzakala, F., and Zdeborová, L. Learning gaussian mixtures with generalized linear models: Precise asymptotics in high-dimensions. In Ranzato, M., Beygelzimer, A., Dauphin, Y., Liang, P., and Vaughan, J. W. (eds.), *Advances in Neural Information Processing Systems*, volume 34, pp. 10144–10157. Curran Associates, Inc., 2021.
- McCullagh, P. *Generalized linear models*. Routledge, 2019.
- Mézard, M., Parisi, G., and Virasoro, M. A. *Spin glass theory and beyond: An Introduction to the Replica Method and Its Applications*, volume 9. World Scientific Publishing Company, 1987.
- Nelder, J. A. and Wedderburn, R. W. Generalized linear models. *Journal of the Royal Statistical Society Series A: Statistics in Society*, 135(3):370–384, 1972.
- Olsson, C., Elhage, N., Nanda, N., Joseph, N., DasSarma, N., Henighan, T., Mann, B., Askell, A., Bai, Y., Chen, A., Conerly, T., Drain, D., Ganguli, D., Hatfield-Dodds, Z., Hernandez, D., Johnston, S., Jones, A., Kernion, J., Lovitt, L., Ndousse, K., Amodei, D., Brown, T., Clark, J., Kaplan, J., McCandlish, S., and Olah, C. In-context learning and induction heads. *Transformer Circuits Thread*, 2022. <https://transformer-circuits.pub/2022/in-context-learning-and-induction-heads/index.html>.
- Parisi, G. Toward a mean field theory for spin glasses. *Physics Letters A*, 73(3):203–205, 1979.
- Parisi, G. Order parameter for spin-glasses. *Physical Review Letters*, 50(24):1946, 1983.
- Paszke, A., Gross, S., Massa, F., Lerer, A., Bradbury, J., Chanan, G., Killeen, T., Lin, Z., Gimelshein, N., Antiga, L., Desmaison, A., Kopf, A., Yang, E., DeVito, Z., Raison, M., Tejani, A., Chilamkurthy, S., Steiner, B., Fang, L., Bai, J., and Chintala, S. Pytorch: An imperative style, high-performance deep learning library. In *Advances in Neural Information Processing Systems 32*, pp. 8024–8035. Curran Associates, Inc., 2019.

- Rangan, S., Schniter, P., Riegler, E., Fletcher, A. K., and Cevher, V. Fixed points of generalized approximate message passing with arbitrary matrices. *IEEE Transactions on Information Theory*, 62(12):7464–7474, 2016.
- Rende, R., Gerace, F., Laio, A., and Goldt, S. Optimal inference of a generalised Potts model by single-layer transformers with factored attention. *arXiv preprint arXiv:2304.07235*, 2023.
- Ruoss, A., Delétang, G., Genewein, T., Grau-Moya, J., Csordás, R., Bennani, M., Legg, S., and Veness, J. Randomized positional encodings boost length generalization of transformers. In Rogers, A., Boyd-Graber, J., and Okazaki, N. (eds.), *Proceedings of the 61st Annual Meeting of the Association for Computational Linguistics (Volume 2: Short Papers)*, pp. 1889–1903, Toronto, Canada, July 2023. Association for Computational Linguistics. doi: 10.18653/v1/2023.acl-short.161.
- Sahiner, A., Ergen, T., Ozturkler, B., Pauly, J., Mardani, M., and Pilanci, M. Unraveling attention via convex duality: Analysis and interpretations of vision transformers. In *International Conference on Machine Learning*, pp. 19050–19088. PMLR, 2022.
- Shaw, P., Uszkoreit, J., and Vaswani, A. Self-Attention with Relative Position Representations. In *Proceedings of the 2018 Conference of the North American Chapter of the Association for Computational Linguistics: Human Language Technologies, Volume 2 (Short Papers)*, pp. 464–468. Association for Computational Linguistics, 2018. doi: 10.18653/v1/N18-2074.
- Sinha, K., Kazemnejad, A., Reddy, S., Pineau, J., Hupkes, D., and Williams, A. The curious case of absolute position embeddings. In Goldberg, Y., Kozareva, Z., and Zhang, Y. (eds.), *Findings of the Association for Computational Linguistics: EMNLP 2022*, pp. 4449–4472, Abu Dhabi, United Arab Emirates, December 2022. Association for Computational Linguistics. doi: 10.18653/v1/2022.findings-emnlp.326.
- Stojnic, M. Meshes that trap random subspaces. *arXiv preprint arXiv:1304.0003*, 2013a.
- Stojnic, M. Upper-bounding l_1 -optimization weak thresholds. *arXiv preprint arXiv:1303.7289*, 2013b.
- Tarzanagh, D. A., Li, Y., Thrampoulidis, C., and Oymak, S. Transformers as support vector machines. *arXiv preprint arXiv:2308.16898*, 2023a.
- Tarzanagh, D. A., Li, Y., Zhang, X., and Oymak, S. Max-margin token selection in attention mechanism. In *Thirty-seventh Conference on Neural Information Processing Systems*, 2023b.
- Thrampoulidis, C., Oymak, S., and Hassibi, B. The gaussian min-max theorem in the presence of convexity. *arXiv preprint arXiv:1408.4837*, 2014.
- Tian, Y., Wang, Y., Chen, B., and Du, S. Scan and snap: Understanding training dynamics and token composition in 1-layer transformer. *arXiv preprint arXiv:2305.16380*, 2023.
- Vaswani, A., Shazeer, N., Parmar, N., Uszkoreit, J., Jones, L., Gomez, A. N., Kaiser, L. u., and Polosukhin, I. Attention is all you need. In Guyon, I., Luxburg, U. V., Bengio, S., Wallach, H., Fergus, R., Vishwanathan, S., and Garnett, R. (eds.), *Advances in Neural Information Processing Systems*, volume 30. Curran Associates, Inc., 2017.
- Von Oswald, J., Niklasson, E., Randazzo, E., Sacramento, J. a., Mordvintsev, A., Zhmoginov, A., and Vladymyrov, M. Transformers learn in-context by gradient descent. In *Proceedings of the 40th International Conference on Machine Learning, ICML’23*. JMLR.org, 2023.
- Weiss, G., Goldberg, Y., and Yahav, E. Thinking like transformers. In Meila, M. and Zhang, T. (eds.), *Proceedings of the 38th International Conference on Machine Learning*, volume 139 of *Proceedings of Machine Learning Research*, pp. 11080–11090. PMLR, 18–24 Jul 2021.
- Zdeborová, L. and Krzakala, F. Statistical physics of inference: Thresholds and algorithms. *Advances in Physics*, 65(5): 453–552, 2016.
- Zhang, R., Frei, S., and Bartlett, P. L. Trained transformers learn linear models in-context. *arXiv preprint arXiv:2306.09927*, 2023.
- Zhong, Z., Liu, Z., Tegmark, M., and Andreas, J. The clock and the pizza: Two stories in mechanistic explanation of neural networks, 2023.

A Technical Details for the Histogram Task

The code for reproducing the results is available at

github.com/SPOC-group/positional-and-semantic-attention.

A.1 Dataset

We use the histogram task as proposed in (Weiss et al., 2021). We consider sequences of fixed length $L = 15$. For every input sequence $\mathbf{x} = [x_1, x_2, \dots, x_L]$ we sample x_i i.i.d. and uniformly from a set of tokens \mathcal{T} of size T , which we set to 15 in our experiments. For visualization purposes we use capitalized letters as tokens. To obtain the target $\mathbf{y} = [y_1, y_2, \dots, y_L]$, we set $y_i = \sum_{j=1}^L \mathbb{1}(x_i = x_j)$, where $\mathbb{1}(b)$ is 1 if the boolean statement b is true and zero otherwise. Therefore, $y_i \in \{1, 2, \dots, L\}$.

A.2 Model

In order to read the input sequence using a transformer we learn an embedding of dimension d for each of the T tokens and L positions, stored in the matrices $E^{\text{token}} = [t_A, t_B, \dots] \in \mathbb{R}^{T \times d}$ and $E^{\text{pos}} = [p_1, p_2, \dots] \in \mathbb{R}^{L \times d}$. We convert the input sequence $\mathbf{x} = [x_1, x_2, \dots, x_L] \in \mathcal{T}^L$ into an embedded sequence $\tilde{\mathbf{x}} \in \mathbb{R}^{L \times d}$ of the same length where $\tilde{x}_i = t_{x_i} + p_i$. This input sequence is then fed into the first layer of the transformer.

Formally, we have

$$\text{logits}_i(\mathbf{x}) = W_2 \text{ReLU}(W_1 \text{LayerNorm}(\text{Attention}_i(\tilde{\mathbf{x}})) + b_1) + b_2 \in \mathbb{R}^c \quad (19)$$

with $W_1 \in \mathbb{R}^{d \times h}$, $b_1 \in \mathbb{R}^h$, $W_2 \in \mathbb{R}^{h \times c}$, $b_2 \in \mathbb{R}^c$. The final prediction is obtained using the argmax on the logits. We have that the score matrix A and the dot-product attention mechanism is

$$\text{Attention}(\mathbf{x}) = A(\mathbf{x})V\mathbf{x} \quad (20)$$

$$A(\mathbf{x}) = \text{Softmax}\left(\frac{\mathbf{x}QK^T\mathbf{x}^T}{\sqrt{d}}\right) \quad (21)$$

where $Q, K, V \in \mathbb{R}^{d \times d}$ and the softmax is applied row-wise. Also, for an $x \in \mathbb{R}^d$ we define

$$\text{LayerNorm}(x) = \frac{x - \mathbb{E}[x]}{\sqrt{\text{Var}(x) + \varepsilon}} * \gamma + \beta \quad (22)$$

where $\gamma, \beta \in \mathbb{R}^d$. We define the empirical loss for a dataset $\mathcal{D} = \{\mathbf{x}^\mu, \mathbf{y}^\mu\}_{\mu=1}^n$ as the average cross entropy loss for all output tokens C , i.e.

$$\mathcal{L}(\mathcal{D}) = \sum_{\mu=1}^n \sum_{l=1}^L - \sum_{c=1}^C [y_l^\mu]_c \log[\text{Softmax}(\text{logits}_l(\mathbf{x}^\mu))]_c. \quad (23)$$

Because of the way in which the histogram dataset is created for a fixed input length L , it follows $C = L$.

A.3 Training procedure and freezing model parameters

To obtain the positional and semantic minima, we set some weights to zero in E^{token} , E^{pos} , Q, K at initialization, and also freeze these zero weights during training. Note that this procedure was used in the literature to study architectural biases of varying model architectures, e.g. by (d'Ascoli et al., 2019) for convolutional neural networks.

With \cdot we denote the initialization that is taken as the default PyTorch initialization for a linear layer. For both semantic and positional initialization, we overwrite this initialization with zeros as follows with $i = 1, \dots, T$ and $j = 1, \dots, L$

$$t_i = \left(\cdot_{d/2} \mid \mathbf{0}_{d/2} \right), \quad p_j = \left(\mathbf{0}_{d/2} \mid \cdot_{d/2} \right), \quad (24)$$

where $\mathbf{0}_{d/2}$ is the all-zero vector of size $d/2$. For the *positional* initialization we additionally set

$$Q = \left(\begin{array}{c|c} \cdot_{d/2 \times d/2} & \mathbf{0}_{d/2 \times d/2} \\ \hline \mathbf{0}_{d/2 \times d/2} & \mathbf{0}_{d/2 \times d/2} \end{array} \right), \quad K = \left(\begin{array}{c|c} \cdot_{d/2 \times d/2} & \mathbf{0}_{d/2 \times d/2} \\ \hline \mathbf{0}_{d/2 \times d/2} & \mathbf{0}_{d/2 \times d/2} \end{array} \right), \quad (25)$$

and for the *semantic* initialization we additionally set

$$Q = \left(\begin{array}{c|c} \mathbf{0}_{d/2 \times d/2} & \mathbf{0}_{d/2 \times d/2} \\ \hline \mathbf{0}_{d/2 \times d/2} & \cdot_{d/2 \times d/2} \end{array} \right), \quad K = \left(\begin{array}{c|c} \mathbf{0}_{d/2 \times d/2} & \mathbf{0}_{d/2 \times d/2} \\ \hline \mathbf{0}_{d/2 \times d/2} & \cdot_{d/2 \times d/2} \end{array} \right), \quad (26)$$

where $\mathbf{0}_{d/2 \times d/2}$ is the all-zero matrix of size $d/2$ by $d/2$. In either case, the attention mechanism only has access to the semantic or positional part of the model.

Training all weights except the ones frozen to zero using Adam on a dataset of size $n = 35,000$, we obtain a $> 99.8\%$ test accuracy on a test set of size $n = 15,000$ for both datasets. We call these parameter configurations θ_{pos} and θ_{sem} respectively (the local minima as referred to in the main text).

In Section 2 in the main text, we show that the attention layer of the two models behaves in qualitatively different ways, by showing the activations of the matrix A for different input sequences.

A.4 Unfreezing model parameters and SGD convergence

Finally, we want to verify that the parameter configurations θ_{pos} and θ_{sem} we obtained using the special initialization and frozen training are stable configurations in the unconstrained parameter space of the model. To show this, we perturb the given parameter configuration slightly using additive Gaussian i.i.d. noise with a scale of 0.001. Subsequently, we run SGD on this perturbed configuration in the unconstrained parameter space for another 100 epochs. We call the parameter configurations obtained after this step $\tilde{\theta}_{pos}$ and $\tilde{\theta}_{sem}$.

While this further training leads the training loss to further decrease and the test accuracy to slightly increase, each models qualitative behaviour before and after extra training remains unchanged, as shown in Fig. 5 and 6, for the examples also used in Fig. 1. The absolute difference in norm between $\tilde{\theta}_{pos}$ and θ_{pos} (respectively $\tilde{\theta}_{sem}$ and θ_{sem}) of parameters is also small (see Table 1).

This evidences, that both resulting parameter configurations are in flat regions of the full parameterization of the transformer model, and that these two regions are further qualitatively different in the same sense that the original ones were. We use this stability in the unconstrained loss landscape as a justification to refer to them as “local minima”.

	$\theta^{\text{init}} \xrightarrow{\text{Adam}} \theta$	$\theta \xrightarrow{\text{SGD}} \tilde{\theta}$
	accuracy θ	$\ \theta^{\text{init}} - \theta\ _2$
positional	0.99885 ± 0.0004	158.85 ± 4.35
semantic	0.99895 ± 0.0012	163.69 ± 8.88

Table 1: Parameter configurations for different types of initializations for the histogram task. Optimizer parameters as in the accompanying code. Average over 10 runs using the same dataset.

B Derivation of Result 4.2

In this Appendix, we provide a detailed derivation of Result 4.2 of the main text. In subsection B.2. we introduce a Generalized Approximate Message Passing algorithm (GAMP) (Rangan et al., 2016). Subsection B.3 then establishes that equations (7) of Result 4.2 track the dynamics of summary statistics describing the GAMP algorithm. In particular, the equations (7) describe the fixed points of GAMP. Finally, subsection B.4 shows that fixed points of GAMP correspond to critical (zero-gradient) points of the empirical loss landscape (3), thus establishing that equations 7 of Result 4.2 describe fixed points of GD.

B.1 Notations

For simplicity, we place ourselves in the setting $r_s = 1$ explored in Section 5 of the main text, but allow the length L of the sentences to be arbitrary, and allow a generic learning model S (2), i.e. not necessarily the dot-product attention model analyzed in Section 5. The case $r_s \geq 2$ follows identical derivation steps, modulo the replacement of all variables by tensor objects. We provide another alternative derivation of Result 4.2 in full generality in Appendix C, using the replica method from statistical physics. Let us note $\{X_\ell\}_{1 \leq \ell \leq L}$ a series of L $n \times d$ matrices, with X_ℓ corresponding to the ℓ -th rows (tokens) of each input sentence x^μ stacked vertically, and normalized by \sqrt{d} . We denote $\tilde{X}_\ell \equiv X_\ell + P_\ell$, where $P \in \mathbb{R}^{n \times d}$ is the matrix with all rows equal to the ℓ -th positional encoding p_ℓ . Let us further define $\rho \in \mathbb{R}^{n \times L \times L}$ the

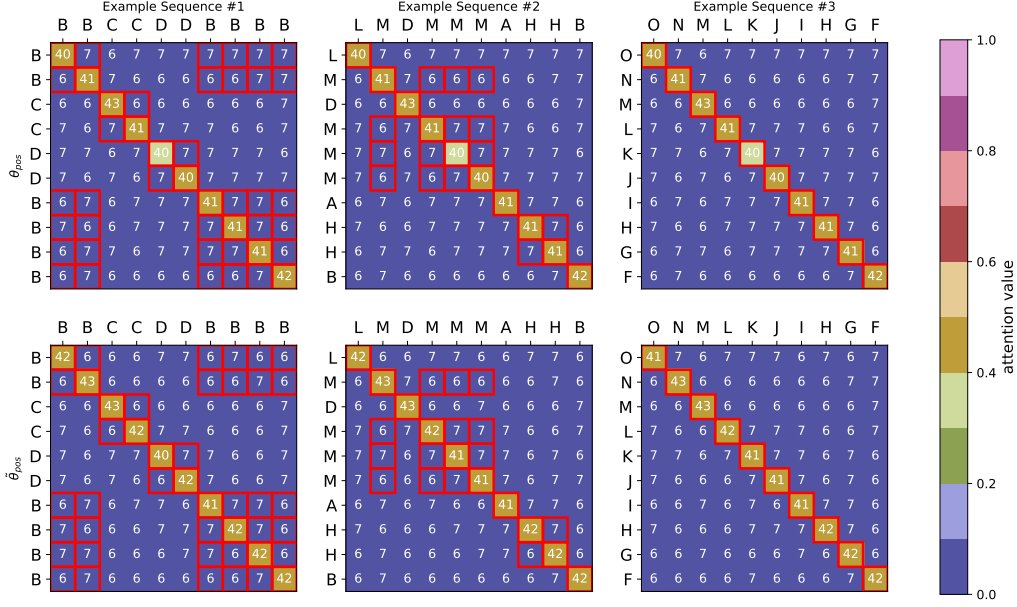


Figure 5: Comparison of the attention layer activations for different sequences for θ_{pos} and $\tilde{\theta}_{pos}$.

tensor corresponding to the sequence of n matrices $\frac{1}{d}x^\mu(x^\mu)^\top \in \mathbb{R}^{L \times L}$. Finally, let us denote $T \in \mathbb{R}^{n \times L \times L}$ the tensor so that the μ -th row of T satisfies $y(x^\mu) = T^\mu x^\mu$, see equation (1). In other words, T corresponds to the concatenation of the target attention matrices.

Before detailing the derivation, we first highlight a simplifying observation. Note that a loss item can be expanded as

$$\begin{aligned} \frac{1}{d} \left\| y(x^\mu) - \mathcal{S} \left[\frac{1}{\sqrt{d}}(x^\mu + p)Q \right] x^\mu \right\|^2 &= \|y(x^\mu)\|^2 + \text{Tr} \mathcal{S} \left[\frac{1}{\sqrt{d}}(x^\mu + p)Q \right] \rho_\Sigma \mathcal{S} \left[\frac{1}{\sqrt{d}}(x^\mu + p)Q \right]^\top \\ &\quad - 2 \text{Tr} \mathcal{T} \left[\frac{1}{\sqrt{d}}x_\ell Q_\star \right] \rho_\Sigma \mathcal{S} \left[\frac{1}{\sqrt{d}}(x_\ell^\mu + p_\ell)Q \right]^\top, \end{aligned} \quad (27)$$

where we used that with high probability in the considered asymptotic limit, for all $1 \leq \mu \leq n$,

$$x x^\top = (x + p)(x + p)^\top = x(x + p)^\top = \rho_\Sigma. \quad (28)$$

Since the first term of (27) does not depend on the weights Q , it can be without loss of generality subtracted from the loss. Without loss of generality, one can thus consider the equivalent empirical risk minimization problem

$$\hat{Q} = \underset{Q \in \mathbb{R}^{d \times r}}{\text{argmin}} \sum_{\mu=1}^n \frac{1}{2d} \left[\text{Tr} \mathcal{S} \left[\frac{1}{\sqrt{d}}(x^\mu + p)Q \right] \rho_\Sigma \mathcal{S} \left[\frac{1}{\sqrt{d}}(x^\mu + p)Q \right]^\top - 2 \text{Tr} \mathcal{T} \left[\frac{1}{\sqrt{d}}x_\ell Q_\star \right] \rho_\Sigma \mathcal{S} \left[\frac{1}{\sqrt{d}}(x_\ell^\mu + p_\ell)Q \right]^\top \right] + \frac{\lambda}{2} \|Q\|^2. \quad (29)$$

The risks (29) and (3) are equivalent, and we shall use the former in the following.

Finally, for arguments $T \in \mathbb{R}^{L \times L}$, $\rho \in \mathbb{R}^{L \times L}$, $\omega \in \mathbb{R}^L$, $V \in \mathbb{R}^{L \times L}$ we introduce the resolvent

$$\begin{aligned} \text{prox}(T, \rho, \omega, V) &\equiv \\ &\underset{x = \{x_\ell \in \mathbb{R}\}_{\ell=1}^L}{\text{arginf}} \left\{ \sum_{\ell, \kappa=1}^L (x_\ell - \omega_\ell)(V^{-1})_{\ell\kappa} (x_\kappa - \omega_\kappa) - 2 \text{Tr} \left[\mathcal{S}[x] \rho T^\top \right] + \text{Tr} \left[\mathcal{S}[x] \rho \mathcal{S}[x]^\top \right] \right\} \end{aligned} \quad (30)$$

Note that the latter part of the bracketed term corresponds to the simplified loss (27) derived in the beginning of Appendix C, which is the one we shall without loss of generality consider in the present appendix. For ease of presentation, we place ourselves under Assumption 4.1, where all the input covariances $\{\Sigma_\ell\}_\ell$ are codiagonalizable. In the following, without loss of generality, we thus assume them diagonal, by placing ourselves in the common basis $\{e_i\}_{1 \leq i \leq d}$ of Assumption 4.1.

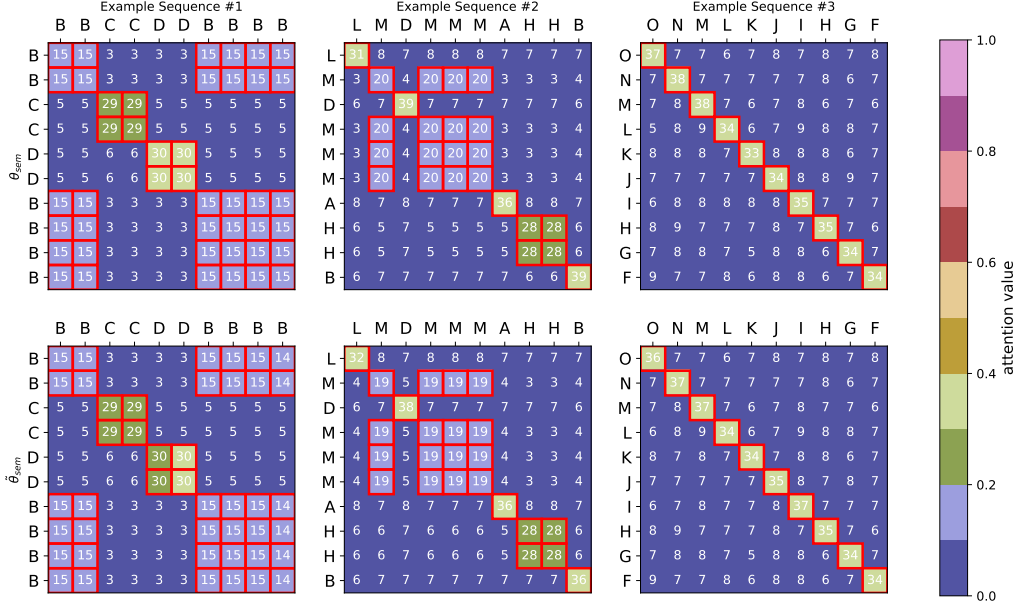


Figure 6: Comparison of the attention layer activations for different sequences for θ_{sem} and $\tilde{\theta}_{sem}$.

B.2 AMP algorithm

We are now in a position to state the AMP algorithm:

Algorithm 1 GAMP

Inputs : $\{\tilde{X}_\ell \in \mathbb{R}^{n \times d}\}_{\ell=1}^L, T \in \mathbb{R}^{n \times L \times L}, \rho \in \mathbb{R}^{n \times L \times L}$

Initialize $\hat{Q}^0 = \sim \mathcal{N}(0, \mathbb{I}_d), \hat{c}^0 = \mathbb{I}_d, \{f_\ell^0 = 0_n\}_{\ell=1}^L$

for $t \leq t_{\max}$ **do**

$$\forall 1 \leq \ell, \kappa \leq L, V_{\ell\kappa}^t = (\tilde{X}_\ell \odot \tilde{X}_\kappa) \hat{c}^t$$

$$\forall 1 \leq \ell \leq L, \omega_\ell^t = \tilde{X}_\ell \hat{Q}^t - \sum_{\kappa=1}^L V_{\ell\kappa}^t f_\kappa^{t-1}$$

$$\forall 1 \leq \ell \leq L, f_\ell^t = \sum_{\kappa} (V^{-1})_{\ell\kappa} (\text{prox}(T, \rho, \omega^t, V^t)_\kappa - \omega_\kappa^t)$$

$$\forall 1 \leq \ell, \kappa \leq L, g_{\ell\kappa}^t = \partial_{\omega_\ell} f_\kappa^t$$

$$A^t = - \sum_{\ell, \kappa=1}^L (\tilde{X}_\ell \odot \tilde{X}_\kappa)^\top g_{\ell\kappa}^t$$

$$b^t = \sum_{\ell=1}^L \tilde{X}_\ell^\top f_\ell^t + A^t \odot \hat{Q}^t$$

$$\hat{Q}^{t+1} = (\lambda \mathbb{I}_d + A^t)^{-1} b^t$$

$$\hat{c}^{t+1} = (\lambda \mathbb{I}_d + A^t)^{-1}$$

end for

return Estimator \hat{Q}

The GAMP algorithm can be derived in standard fashion from the Belief Propagation (BP) algorithm, see e.g. (Rangan et al., 2016; Bayati & Montanari, 2011a) or (Zdeborová & Krzakala, 2016) for an overview. Compared to the standard GAMP iterations for Generalized linear models, one needs to account for the fact that there exist different sources of data \tilde{X}_ℓ (corresponding to the ℓ -th tokens of each input sentence), and for the fact that the output of the equivalent GLM are $\mathbb{R}^{L \times L}$ -valued attention matrices. In the following subsection, we show that the fixed points of GAMP 1 correspond to critical points of the empirical loss (3), i.e. fixed points of Gradient Descent (GD), allowing to connect Result 4.2 to our numerical experiments using GD.

B.3 State evolution

In this section we show that the dynamics of the GAMP Algorithm 1 are tracked by the summary statistics of Result 4.2. In particular, the equations (7) describe the statistics of the GAMP fixed points. To see this, it is convenient to take as a starting point the relaxed Belief Propagation (rBP) equations, which are a step upstream in the derivation of the GAMP iterations, and which are asymptotically equivalent– see e.g. (Zdeborová & Krzakala, 2016) for a review or e.g. (Clarté et al., 2023), Appendix A, for a detailed walkthrough. The rBP equations read

Algorithm 2 rBP

Inputs : $\{\tilde{X}_\ell \in \mathbb{R}^{n \times d}\}_{\ell=1}^L, T \in \mathbb{R}^{n \times L \times L}, \rho \in \mathbb{R}^{n \times L \times L}$

Initialize $\forall 1 \leq \mu \leq n, 1 \leq i \leq d, \hat{Q}_{i \rightarrow \mu}^0 = 0, \hat{c}_{i \rightarrow \mu}^0 = 1, \{f_{\ell \mu \rightarrow i}^0 = 0\}_{\ell=1}^L$

for $t \leq t_{\max}$ **do**

$$\forall 1 \leq \ell, \kappa \leq L, 1 \leq \mu \leq n, 1 \leq i \leq d, (V_{\mu \rightarrow i}^t)_{\ell \kappa} = \sum_{j \neq i} (\tilde{x}_{\ell j}^\mu) (\tilde{x}_{\kappa j}^\mu) \hat{c}_{j \rightarrow \mu}^t$$

$$\forall 1 \leq \ell, 1 \leq \mu \leq n, 1 \leq i \leq d, \omega_{\ell, \mu \rightarrow i}^t = \sum_{j \neq i} \tilde{x}_{\ell, i}^\mu \hat{Q}_{j \rightarrow \mu}$$

$$\forall 1 \leq \ell, 1 \leq \mu \leq n, 1 \leq i \leq d, f_{\ell, \mu \rightarrow i}^t = \sum_{\kappa} (V_{\mu \rightarrow i}^{-1})_{\ell \kappa} (\text{prox}(T_\mu, \rho_\mu, \omega_{\mu \rightarrow i}^t, V_{\mu \rightarrow i}^t)_{\kappa} - \omega_{\kappa, \mu \rightarrow i}^t)$$

$$\forall 1 \leq \ell, \kappa \leq L, 1 \leq \mu \leq n, 1 \leq i \leq d, g_{\ell \kappa, \mu \rightarrow i}^t = \partial_{\omega_\ell} f_{\kappa \mu \rightarrow i}^t$$

$$\forall 1 \leq \mu \leq n, 1 \leq i \leq d, A_{i \rightarrow \mu}^t = - \sum_{\ell, \kappa=1}^L \sum_{\nu \neq \mu} (\tilde{x}_{\ell i}^\nu) (\tilde{x}_{\kappa i}^\nu) g_{\ell \kappa, \nu \rightarrow i}^t$$

$$\forall 1 \leq \mu \leq n, 1 \leq i \leq d, b_{i \rightarrow \mu}^t = \sum_{\ell=1}^L \sum_{\nu \neq \mu} x_{\ell i}^\nu f_{\ell, \nu \rightarrow i}^t$$

$$\forall 1 \leq \mu \leq n, 1 \leq i \leq d, \hat{Q}_{i \rightarrow \mu}^{t+1} = (\lambda \mathbb{I}_d + A_{i \rightarrow \mu}^t)^{-1} b_{i \rightarrow \mu}^t$$

$$\forall 1 \leq \mu \leq n, 1 \leq i \leq d, \hat{c}_{i \rightarrow \mu}^{t+1} = (\lambda \mathbb{I}_d + A_{i \rightarrow \mu}^t)^{-1}$$

end for

return Estimator \hat{Q}

As conventional, we note \cdot_μ the version of a variable $\cdot_{\mu \rightarrow i}$ where the summation also encompasses the index i , and \cdot_i the version of a variable $\cdot_{i \rightarrow \mu}$ where the summation also encompasses the index μ . Note that in all cases above the two variables differ by at most $\Theta_d(1/\sqrt{d})$.

Concentration of $(V_{\mu \rightarrow i}^t)_{\ell \kappa}$ We first study the statistics of $V_{\mu \rightarrow i}^t, A_{i \rightarrow \mu}^t$, remembering that the data $\tilde{x}_{\ell i}^\mu \equiv (x_\ell^\mu)_i / \sqrt{d} + (p_\ell)_i / \sqrt{d}$ in the notation of the main text, with $(x_\ell^\mu)_i = \Theta_d(1), (p_\ell)_i = \Theta_d(1/\sqrt{d})$. Replacing in the rBP updates:

$$\begin{aligned} (V_{\mu \rightarrow i}^t)_{\ell \kappa} &= \sum_{j \neq i} (\tilde{x}_{\ell j}^\mu) (\tilde{x}_{\kappa j}^\mu) \hat{c}_{j \rightarrow \mu}^t \\ &= \underbrace{\frac{1}{d} \sum_{j \neq i} (x_\ell^\mu)_j (x_\kappa^\mu)_j \hat{c}_{j \rightarrow \mu}^t}_{\delta_{\ell \kappa} \Theta_d(1) + (1 - \delta_{\ell \kappa}) \Theta_d(1/\sqrt{d})} + \underbrace{\frac{1}{d} \sum_{j \neq i} (x_\ell^\mu)_j (p_\kappa)_j \hat{c}_{j \rightarrow \mu}^t}_{\Theta_d(1/d)} + (\ell \leftrightarrow \kappa) + \underbrace{\frac{1}{d} \sum_{j \neq i} (p_\ell)_j (p_\kappa)_j \hat{c}_{j \rightarrow \mu}^t}_{\Theta_d(1/d)} \\ &= \delta_{\ell \kappa} \frac{1}{d} \sum_j (\Sigma_\ell)_{jj} \hat{c}_j^t \equiv V_\ell^t \end{aligned} \quad (31)$$

Distribution of $\omega_{\ell, \mu \rightarrow i}^t$ Let us first introduce the teacher local field

$$h_{\mu, \ell} = \sum_i (x_\ell^\mu)_i Q_i^* \quad (32)$$

Like e.g. (Clarté et al., 2023), Appendix A, we first ascertain the joint distribution of $h_{\mu, \ell}, \omega_{\ell, \mu \rightarrow i}^t$ with respect to the data. These variables have mean

$$\mathbb{E}[\omega_{\ell, \mu \rightarrow i}^t] = \frac{p_\ell^\top \hat{Q}^t}{\sqrt{d}} \equiv m_\ell^t \quad (33)$$

and respective variance

$$\mathbb{V}[\omega_{\ell, \mu \rightarrow i}^t \omega_{\kappa, \nu \rightarrow j}^t] = \delta_{\mu\nu} \delta_{\ell\kappa} \frac{1}{d} \sum_{i,j} \hat{Q}_i^t(\Sigma_\ell)_{ij} \hat{Q}_j^t \equiv \delta_{\mu\nu} \delta_{\ell\kappa} q_\ell^t \quad (34)$$

$$\mathbb{E}[h_{\mu\ell} h_{\nu\kappa}] = \delta_{\mu\nu} \delta_{\ell\kappa} \frac{1}{d} \sum_{i,j} Q_i^*(\Sigma_\ell)_{ij} Q_j^* \equiv \delta_{\mu\nu} \delta_{\ell\kappa} \rho_\ell \quad (35)$$

$$\mathbb{E}[h_{\mu\ell} \omega_{\kappa, \nu \rightarrow j}^t] = \delta_{\mu\nu} \delta_{\ell\kappa} \frac{1}{d} \sum_{i,j} Q_i^*(\Sigma_\ell)_{ij} \hat{Q}_j^t \equiv \delta_{\mu\nu} \delta_{\ell\kappa} \theta_\ell^t \quad (36)$$

Distribution of $b_{i \rightarrow \mu}^t$ Let us ascertain the distribution of $b_{i \rightarrow \mu}^t$.

$$\begin{aligned} b_{i \rightarrow \mu}^t &= \sum_{\ell} \sum_{\nu \neq \mu} (\tilde{x}_\ell^\nu)_i (V_\ell^t)^{-1} \underbrace{\left(\text{prox}(T_\nu, \rho_\nu, \{\omega_{\kappa, \nu \rightarrow i}^t\}_\kappa, V_{\nu \rightarrow i}^t) \right)_\ell - \omega_{\ell, \nu \rightarrow i}^t}_{\equiv \text{prox}(T_\nu, \rho_\nu, \{\omega_{\kappa, \nu \rightarrow i}^t\}_\kappa, V_{\nu \rightarrow i}^t)_\ell} \\ &= \sum_{\ell} \sum_{\nu \neq \mu} \frac{1}{\sqrt{d}} \left[(x_\ell^\nu)_i + (p_\ell)_i \right] \left[\text{prox}(\mathbb{T}[\{h_{\nu \rightarrow i, \kappa}\}_\kappa], \rho_\nu, \{\omega_{\kappa, \nu \rightarrow i}^t\}_\kappa, V_{\nu \rightarrow i}^t)_\ell \right. \\ &\quad \left. + \frac{1}{\sqrt{d}} \sum_{\gamma} (x_\ell^\nu)_i Q_i^* \partial_{h_\gamma} \text{prox}(\mathbb{T}[\{h_{\nu \rightarrow i, \kappa}\}_\kappa], \rho_\nu, \{\omega_{\kappa, \nu \rightarrow i}^t\}_\kappa, V_{\nu \rightarrow i}^t)_\ell \right], \end{aligned} \quad (37)$$

leading asymptotically to

$$\begin{aligned} \mathbb{E}[b_{i \rightarrow \mu}^t] &= \sum_{\ell} (\sqrt{d} p_\ell)_i \underbrace{\alpha \mathbb{E}_{H=\{h_\kappa\} \Xi = \{\xi_\kappa\}} \text{prox}(\mathbb{T}[H], \rho_\Sigma, \{m_\kappa^t + \sqrt{q_\kappa^t} \xi_\kappa\}_\kappa, \{V_\kappa^t\}_\kappa)_\ell}_{\equiv \hat{m}_\ell^t} \\ &\quad + Q_i^* \sum_{\ell} (\Sigma_\ell)_{ii} \underbrace{\alpha \mathbb{E}_{H, \Xi} \partial_{h_\ell} \text{prox}(\mathbb{T}[H], \rho_\Sigma, \{m_\kappa^t + \sqrt{q_\kappa^t} \xi_\kappa\}_\kappa, \{V_\kappa^t\}_\kappa)_\ell}_{\equiv \hat{\theta}_\ell^t} \end{aligned} \quad (38)$$

where the expectations bear over $\xi_\ell \sim \mathcal{N}(0, 1)$ and $h_\ell \sim \mathcal{N}(\xi_\ell \theta_\ell^t / \sqrt{q_\ell^t}, \rho_\ell - (\theta_\ell^t)^2 / q_\ell^t)$. The variance is given by

$$\mathbb{V}[b_i^t, b_j^t] = \delta_{ij} \sum_{\ell} (\Sigma_\ell)_{ii} \underbrace{\alpha \mathbb{E}_{H, \Xi} \text{prox}(\mathbb{T}[H], \rho_\Sigma, \{m_\kappa^t + \sqrt{q_\kappa^t} \xi_\kappa\}_\kappa, \{V_\kappa^t\}_\kappa)_\ell^2}_{\equiv \hat{q}_\ell^t} \quad (39)$$

Concentration of $A_{i \rightarrow \mu}^t$ Similarly to the derivation for $V_{\mu \rightarrow i}^t$, $A_{i \rightarrow \mu}^t$ concentrates to

$$A_{i \rightarrow \mu}^t = \sum_{\ell} \underbrace{-\alpha \frac{1}{V_\ell^t} \left(\mathbb{E}_{H, \Xi} \partial_{\omega_\ell} \text{prox}(\mathbb{T}[H], \rho_\Sigma, \{m_\kappa^t + \sqrt{q_\kappa^t} \xi_\kappa\}_\kappa, \{V_\kappa^t\}_\kappa)_\ell - 1 \right)}_{\equiv \hat{V}_\ell^t} (\Sigma_\ell)_{ii} \quad (40)$$

Recovering Result 4.2 Wrapping up, we now massage these equations to recover equations (7) from Result 4.2 of the main text. Starting from (31):

$$\begin{aligned} V_\ell^t &= \frac{1}{d} \sum_j (\Sigma_\ell)_{jj} \frac{1}{\lambda + \sum_{\kappa} \hat{V}_\kappa^{t-1}(\Sigma_\kappa)} \\ &= \int d\nu(\gamma, \tau) \gamma_\ell \left(\lambda + \sum_{\kappa} \hat{V}_\kappa^{t-1} \gamma_\kappa \right)^{-1}. \end{aligned} \quad (41)$$

Next, for q_ℓ^t (34):

$$\begin{aligned} q_\ell^t &= \frac{1}{d} \sum_i (\Sigma_\ell)_{ii} \left(\left(\sum_{\kappa} (\sqrt{d} (p_\kappa)_i \hat{m}_\kappa^{t-1} + Q_i^*(\Sigma_\kappa)_{ii} \hat{\theta}_\kappa) \right)^2 + (\Sigma_\kappa)_{ii} \hat{q}_\kappa^{t-1} \right) \left(\lambda + \sum_{\kappa} \hat{V}_\kappa^{t-1}(\Sigma_\kappa) \right)^{-2} \\ &= \int d\nu(\gamma, \tau, \pi) \gamma_\ell \left(\left(\sum_{\kappa} \hat{m}_\kappa^{t-1} \tau_\kappa + \hat{\theta}_\kappa \gamma_\kappa \pi_\kappa \right)^2 + \gamma_\kappa \hat{q}_\kappa^{t-1} \right) \left(\lambda + \sum_{\kappa} \hat{V}_\kappa^{t-1} \gamma_\kappa \right)^{-2} \end{aligned} \quad (42)$$

For θ_ℓ^t (34):

$$\begin{aligned}\theta_\ell^t &= \frac{1}{d} \sum_1 (\Sigma_\ell)_{ii} Q_i^* \left(\sum_\kappa (\sqrt{d}(p_\kappa)_i \hat{m}_\kappa^{t-1} + Q_i^*(\Sigma_\kappa)_{ii} \hat{\theta}_\kappa) \left(\lambda + \sum_\kappa \hat{V}_\kappa^{t-1}(\Sigma_\kappa) \right)^{-1} + o_d(1) \right) \\ &= \int d\nu(\gamma, \tau, \pi) \gamma_\ell \pi_\ell \left(\sum_\kappa \hat{m}_\kappa^{t-1} \tau_\kappa + \hat{\theta}_\kappa \gamma_\kappa \pi_\kappa \right) \left(\lambda + \sum_\kappa \hat{V}_\kappa^{t-1} \gamma_\kappa \right)^{-1}.\end{aligned}\quad (43)$$

Finally for m_ℓ^t (33):

$$\begin{aligned}m_\ell^t &= \frac{1}{d} \sum_i (\sqrt{d} p_\ell)_i \left(\sum_\kappa (\sqrt{d}(p_\kappa)_i \hat{m}_\kappa^{t-1} + Q_i^*(\Sigma_\kappa)_{ii} \hat{\theta}_\kappa) \left(\lambda + \sum_\kappa \hat{V}_\kappa^{t-1}(\Sigma_\kappa) \right)^{-1} + o_d(1) \right) \\ &= \int d\nu(\gamma, \tau, \pi) \tau_\ell \left(\sum_\kappa \hat{m}_\kappa^{t-1} \tau_\kappa + \hat{\theta}_\kappa \gamma_\kappa \pi_\kappa \right) \left(\lambda + \sum_\kappa \hat{V}_\kappa^{t-1} \gamma_\kappa \right)^{-1}.\end{aligned}\quad (44)$$

For \hat{m}_ℓ^t (38):

$$\hat{m}_\ell^t = \alpha \mathbb{E}_{H, \Xi} \frac{1}{V_\ell^t} \left[\text{prox}_\ell - \sqrt{q_\ell^t} \xi_\ell - m_\ell^t \right], \quad (45)$$

while for $\hat{\theta}_\ell^t$ (38):

$$\begin{aligned}\hat{\theta}_\ell^t &= \alpha \mathbb{E}_{H, \Xi} \frac{1}{V_\ell^t} \partial_{h_\ell} \left[\text{prox}_\ell - \sqrt{q_\ell^t} \xi_\ell - m_\ell^t \right] \\ &= \alpha \mathbb{E}_{H, \Xi} \frac{1}{V_\ell^t} \frac{h_\ell - \theta_\ell^t / \sqrt{q_\ell^t} \xi_\ell}{\rho_\ell - (\theta_\ell^t)^2 / q_\ell^t} \left[\text{prox}_\ell - \sqrt{q_\ell^t} \xi_\ell - m_\ell^t \right].\end{aligned}\quad (46)$$

Now turning to \hat{q}_ℓ^t :

$$\hat{q}_\ell^t = \alpha \mathbb{E}_{H, \Xi} \left[\left(\frac{1}{V_\ell^t} \text{prox}_\ell - \sqrt{q_\ell^t} \xi_\ell - m_\ell^t \right)^2 \right]. \quad (47)$$

Finally, for \hat{V}_ℓ^t (40):

$$\begin{aligned}\hat{V}_\ell^t &= -\alpha \mathbb{E}_{H, \Xi} \frac{1}{V_\ell^t} [\partial_{\omega_\ell} \text{prox}_\ell - 1] \\ &= -\alpha \mathbb{E}_{H, \Xi} \frac{1}{V_\ell^t} \left[\frac{1}{\sqrt{q_\ell^t}} \partial_\xi (\text{prox}_\ell - \sqrt{q_\ell^t} \xi_\ell - m_\ell) \right] \\ &= \alpha \mathbb{E}_{H, \Xi} \frac{1}{\sqrt{q_\ell^t} V_\ell^t} \left[\frac{\theta_\ell^t}{\sqrt{q_\ell^t} V_\ell^t} \left(\frac{h_\ell - \sqrt{q_\ell^t} \xi_\ell}{\rho_\ell - (\theta_\ell^t)^2 / q_\ell^t} - \xi \right) (\text{prox}_\ell - \sqrt{q_\ell^t} \xi_\ell - m_\ell) \right] \\ &= \frac{\theta_\ell^t \hat{\theta}_\ell^t}{q_\ell^t} - \alpha \mathbb{E}_{H, \Xi} \frac{1}{\sqrt{q_\ell^t} V_\ell^t} (\text{prox}_\ell - \sqrt{q_\ell^t} \xi_\ell - m_\ell) \xi_\ell\end{aligned}\quad (48)$$

Summary : State evolution equations The state evolution equations asymptotically describing the dynamics of the GAMP algorithm 1 thus read

$$\begin{cases} V_\ell^t = \int d\nu(\gamma, \tau) \gamma_\ell \left(\lambda + \sum_{\kappa} \hat{V}_\kappa^{t-1} \gamma_\kappa \right)^{-1} \\ q_\ell^t = \int d\nu(\gamma, \tau, \pi) \gamma_\ell \left(\left(\sum_{\kappa} \hat{m}_\kappa^{t-1} \tau_\kappa + \hat{\theta}_\kappa \gamma_\kappa \pi_\kappa \right)^2 + \gamma_\kappa \hat{q}_\kappa^{t-1} \right) \left(\lambda + \sum_{\kappa} \hat{V}_\kappa^{t-1} \gamma_\kappa \right)^{-2} \\ \theta_\ell^t = \int d\nu(\gamma, \tau, \pi) \gamma_\ell \pi_\ell \left(\sum_{\kappa} \hat{m}_\kappa^{t-1} \tau_\kappa + \hat{\theta}_\kappa \gamma_\kappa \pi_\kappa \right) \left(\lambda + \sum_{\kappa} \hat{V}_\kappa^{t-1} \gamma_\kappa \right)^{-1} \\ m_\ell^t = \int d\nu(\gamma, \tau, \pi) \tau_\ell \left(\sum_{\kappa} \hat{m}_\kappa^{t-1} \tau_\kappa + \hat{\theta}_\kappa \gamma_\kappa \pi_\kappa \right) \left(\lambda + \sum_{\kappa} \hat{V}_\kappa^{t-1} \gamma_\kappa \right)^{-1} \end{cases} \quad (49)$$

$$\begin{cases} \hat{V}_\ell^t = \frac{\theta_\ell^t \hat{\theta}_\ell^t}{q_\ell^t} - \alpha \mathbb{E}_{H, \Xi} \frac{1}{\sqrt{q_\ell^t} V_\ell^t} (\text{prox}_\ell - \sqrt{q_\ell^t} \xi_\ell - m_\ell) \xi_\ell \\ \hat{q}_\ell^t = \alpha \mathbb{E}_{H, \Xi} \left[\left(\frac{1}{\sqrt{V_\ell^t}} \text{prox}_\ell - \sqrt{q_\ell^t} \xi_\ell - m_\ell^t \right)^2 \right] \\ \hat{\theta}_\ell^t = \alpha \mathbb{E}_{H, \Xi} \frac{1}{\sqrt{V_\ell^t}} \frac{h_\ell - \theta_\ell^t / \sqrt{q_\ell^t} \xi_\ell}{\rho_\ell - (\theta_\ell^t)^2 / q_\ell^t} \left[\text{prox}_\ell - \sqrt{q_\ell^t} \xi_\ell - m_\ell^t \right] \\ \hat{m}_\ell^t = \alpha \mathbb{E}_{H, \Xi} \frac{1}{\sqrt{V_\ell^t}} \left[\text{prox}_\ell - \sqrt{q_\ell^t} \xi_\ell - m_\ell^t \right] \end{cases} \quad (50)$$

which exactly recovers equations (7) of Result 4.2 of the main text, for the case $r_s = 1$ considered in the present Appendix. Again, we mention that the case $r_s \geq 2$ should follow straightforwardly with the exact same derivation steps, using tensor variables (see e.g. (Cornacchia et al., 2023)). This subsection has thus established that the equations (7) (with time indices) describe the summary statistics capturing the dynamics of GAMP iterations 1. In particular, (7) describe the fixed points of GAMP. The next subsection further shows that the (stable) fixed points of GAMP correspond to critical (zero-gradient) points of the empirical landscape (3), i.e. fixed points of gradient descent. Finally, we provide in Appendix C an alternative derivation of the state evolution equations (7)(49), using the replica method from statistical physics (Parisi, 1979, 1983).

B.4 Fixed points of GAMP are fixed points of GD

In this subsection, we show that fixed points of GAMP 1, as asymptotically described by (7) in Result 4.2, correspond to critical (zero gradient) points of the empirical landscape (3). Again, we present the result for $r_s = 1$ for clarity, the generalization to $r_s \geq 2$ being straightforward (see e.g. (Cornacchia et al., 2023)). In the previous notations, let us denote the (simplified, see (27)) empirical loss as

$$L(\{\tilde{X}_\ell Q\}_\ell) + g(Q) \quad (51)$$

where we introduced the shorthands

$$L(\{h_\ell\} \in \mathbb{R}^n) \equiv \sum_{\mu=1}^n \left(-2 \text{Tr} \left[\mathbf{S}[\{h_\ell^\mu\}_\ell] \rho_\mu T_\mu^\top \right] + \text{Tr} \left[\mathbf{S}[\{h_\ell^\mu\}_\ell] \rho_\mu \mathbf{S}[\{h_\ell^\mu\}_\ell]^\top \right] \right) \quad (52)$$

$$g(Q) \equiv \frac{\lambda}{2} \|Q\|^2, \quad (53)$$

i.e. respectively the simplified empirical loss (3) and the regularization, as functions with matrix arguments. The empirical minimization problem (3) can thus be written compactly as

$$\hat{Q} = \underset{Q \in \mathbb{R}^d}{\text{argmin}} \left\{ L(\{\tilde{X}_\ell Q\}_\ell) + r(Q) \right\} \quad (54)$$

with the critical (zero-gradient) condition being given by

$$\sum_{\ell=1}^L \tilde{X}_\ell^\top \partial_\ell L(\{\tilde{X}_\ell Q\}_\ell) + \partial g(Q) \stackrel{!}{=} 0. \quad (55)$$

Let us choose a diagonal definite $A \in \mathbb{R}^{d \times d}$, and a sequence $\{V_\mu\}_{1 \leq \mu \leq n}$ of symmetric definite $L \times L$ matrices. Group them into a block diagonal matrix $\tilde{V} \in \mathbb{R}^{Ln \times Ln}$, so that the μ -th block of \tilde{V} corresponds to V_μ . It shall prove useful

to further introduce the matrices $\check{X} \in \mathbb{R}^{d \times nL}$ (resp. $\check{\partial}L(\check{X}) \in \mathbb{R}^{nL}$), defined as the concatenation of the matrices $\check{X}_1, \dots, \check{X}_L$ (resp. $\partial_1 L, \dots, \partial_L L$), viewed as n blocks of length L . Then without loss of generality the zero-gradient condition can be rewritten as

$$\check{X}^\top V^{-1} \left(V \check{\partial}L(\check{X}) - \check{X}Q \right) + A(A^{-1} \partial g(Q) + Q) \stackrel{!}{=} \check{X}^\top V^{-1} \check{X}Q + AQ. \quad (56)$$

Similarly to (Cornacchia et al., 2023), let us introduce

$$\check{\omega} \equiv V \check{\partial}L(\check{X}) - \check{X}Q. \quad (57)$$

This can be written in terms of a resolvent as

$$\check{X}Q = \text{prox}(\check{\omega}) \quad (58)$$

where

$$\text{prox}(\check{\omega}) \in \mathbb{R}^{nL} = \underset{\check{x} \in \mathbb{R}^{nL}}{\text{argmin}} \left\{ \frac{1}{2} \|\check{x} - \check{\omega}\|_V^2 + L(\check{x}) \right\} \quad (59)$$

which corresponds to (30). Similarly, we denote

$$b \equiv A^{-1} \partial g(Q) + Q \quad (60)$$

So that

$$Q = \text{prox}_g(b) = \underset{x \in \mathbb{R}^d}{\text{argmin}} \left\{ \frac{1}{2} \|x - b\|_{A^{-1}}^2 + g(x) \right\} \quad (61)$$

In the particular case of an ℓ_2 regularization $g(\cdot) = \lambda/2 \|\cdot\|^2$, note that

$$\text{prox}_g(b) = (\lambda \mathbb{I}_d + A)^{-1} Ab. \quad (62)$$

The zero-gradient condition can now be rewritten as

$$\begin{cases} \check{X}^\top V^{-1} (\text{prox}(\check{\omega}) - \check{\omega}) = A(b - \text{prox}_g(b)) \\ \check{X} \text{prox}_g(b) = \text{prox}(\check{\omega}) \end{cases} \quad (63)$$

One is now in a position to expand the concatenated variables $\check{\cdot}$ into a sequence of L n -dimensional parameters. For $u = \text{prox}(\check{\omega}), \check{\omega}$ let us denote $u_{\mu\ell}$ ($1 \leq \mu \leq n, 1 \leq \ell \leq L$) the ℓ -th component of the μ -th block. Introduce

$$f_{\mu\ell} \equiv \sum_{\kappa} (V_{\mu}^{-1})_{\ell\kappa} (\text{prox}(\check{\omega})_{\mu\kappa} - \check{\omega}_{\mu\kappa}). \quad (64)$$

Denote $f_{\ell} \equiv (f_{\mu\ell})_{1 \leq \mu \leq n} \in \mathbb{R}^n, \omega_{\ell} \equiv (\omega_{\mu\ell})_{1 \leq \mu \leq n} \in \mathbb{R}^n$. The system of equations (63) can then be rewritten as (further redefining $b \leftarrow Ab$):

$$\begin{cases} \sum_{\ell} \check{X}_{\ell}^\top f_{\ell} = b - A(\lambda \mathbb{I}_d + A)^{-1} b \\ \check{X}_{\ell} (\lambda \mathbb{I}_d + A)^{-1} b = \sum_{\kappa} V_{\ell\kappa} f_{\kappa} - \omega_{\ell} \end{cases} \quad (65)$$

We used the assumption that $g(\cdot)$ is an ℓ_2 regularization. Finally, introducing $\hat{Q} = \text{prox}_g(A^{-1}b) = (\lambda \mathbb{I}_d + A)^{-1} b$, one reaches

$$\begin{cases} \sum_{\ell} \check{X}_{\ell}^\top f_{\ell} = b - A\hat{Q} \\ \check{X}_{\ell} \hat{Q} = \sum_{\kappa} V_{\ell\kappa} f_{\kappa} - \omega_{\ell} \end{cases} \quad (66)$$

which corresponds to the fixed-point equations of GAMP (Algorithm 1). This finishes to show the correspondence between the fixed points of GAMP and the critical points of the empirical landscape (3). To summarize, we have shown that equations (7) describe the zero-gradient points of the empirical loss landscape (3), i.e. fixed points of GD.

B.5 Towards a rigorous proof of result 4.2

While the connection between the GAMP fixed point and the extrema of the loss is sound, and has been at the roots of many rigorous results for convex losses, see e.g. (Bayati & Montanari, 2011b; Donoho & Montanari, 2016; Emami et al., 2020; Loureiro et al., 2021; Gerbelot et al., 2022), there exist technical difficulties in adapting these rigorous arguments to the present setting, and a fully rigorous proof would warrant sizable work. While we leave this challenging task for future work, we wish to discuss how it can be potentially achieved. The first task would require the proof of point-wise convergence of GAMP, as indeed, the identification of the GAMP estimates with the one of the extrema of the loss function requires to be at the fixed point of the iteration. This difficulty, discussed in detail in, e.g. (Bolthausen, 2014; Loureiro et al., 2021; Gerbelot et al., 2022), can be in principle addressed by computing the convergence criterion from the state evolution equations (see (Bolthausen, 2014) the discussion in Lemma 7 in (Gerbelot et al., 2022)), a criterion sometimes called the "replicon" in the context of replica theory (Mézard et al., 1987).

Provided the replicon criterion is satisfied, all converging fixed point described by our theory thus correspond rigorously to fixed point of the loss. The last task would be to prove that the minimum of the loss is indeed the fixed point we found with minimum energy. A potential strategy to prove this would be to use the Gordon-Minimax approach of (Gordon, 1988). While it is used in many situations for convex problems (e.g. (Thrapoulidis et al., 2014; Stojnic, 2013a,b)), only one side would be required for our (non-convex) problem thanks to the GAMP matching bound. We hope that our results would provide inspiration for further research in this direction.

C Derivation of Result 4.2 with the replica method

In the Appendix we provide an alternative derivation of Result 4.2, which sharply characterizes the global minimum of the empirical loss (3), using the heuristic replica method from statistical physics (Parisi, 1979, 1983) in its replica-symmetric formulation. First observe that for any test function $\phi(\hat{Q})$ of the minimizer \hat{Q} of (3),

$$\phi(\hat{Q}) = \lim_{\beta \rightarrow \infty} \mathbb{E}_{\mathcal{D}} \frac{1}{Z} \int dQ \phi(Q) e^{-\beta \mathcal{R}[Q]}, \quad (67)$$

where we denoted $R[Q]$ the empirical loss (3), and

$$Z \equiv \int dQ e^{-\beta \mathcal{R}[Q]} \quad (68)$$

the normalization factor, also known as the *partition function* in statistical physics. We remind that \mathcal{D} refers to the training set. In order to access key summary statistics and learning metrics associated to \hat{Q} , it is therefore reasonable to seek to compute the generating function associated to the measure (67), namely $\mathbb{E} \ln Z$. Such computations can be addressed using the *replica* method from statistical physics (Parisi, 1979, 1983), building on the identity

$$\ln Z = \lim_{s \rightarrow 0} \frac{Z^s - 1}{s}. \quad (69)$$

The backbone of the derivation thus lies in the computation of $\mathbb{E} Z^s$. Below, we detail the derivation for a generic convex regularizer $g : \mathbb{R}^d \rightarrow \mathbb{R}_+$ and later specialize to the case of ℓ_2 regularization. The replicated partition function thus reads

$$\mathbb{E} Z^s = \int \prod_{a=1}^s dQ_a e^{-\beta \sum_{a=1}^s g(Q_a)} \prod_{\mu=1}^n \mathbb{E}_x e^{-\beta \sum_{a=1}^s \left(\text{Tr} \mathbb{S} \left[\frac{1}{\sqrt{d}} (x+p) Q_a \right] \rho_{\Sigma} \mathbb{S} \left[\frac{1}{\sqrt{d}} (x+p) Q_a \right]^{\top} - 2 \text{Tr} \mathbb{T} \left[\frac{1}{\sqrt{d}} x_{\ell} Q_{\star} \right] \rho_{\Sigma} \mathbb{S} \left[\frac{1}{\sqrt{d}} (x+p) Q_a \right]^{\top} \right)}. \quad (70)$$

Introduce the local fields

$$h^a \equiv \frac{x Q_a}{\sqrt{d}} \in \mathbb{R}^{L \times r}, \quad h^{\star} \equiv \frac{x Q_{\star}}{\sqrt{d}} \in \mathbb{R}^{L \times t} \quad (71)$$

and the overlaps

$$m_a \equiv \frac{p Q_a}{\sqrt{d}} \in \mathbb{R}^{L \times r}, \quad (72)$$

with rows m_a^ℓ . These fields have statistics

$$\mathbb{E}_x[h_\ell^a(h_\kappa^b)^\top] = \delta_{\ell\kappa} \frac{Q_a^\top \Sigma_\ell Q_b}{d} \equiv q_{ab}^\ell \quad (73)$$

$$\mathbb{E}_x[h_\ell^*(h_\kappa^*)^\top] = \delta_{\ell\kappa} \frac{Q_\star^\top \Sigma_\ell Q_\star}{d} \equiv \rho_\ell \quad (74)$$

$$\mathbb{E}_x[h_\ell^a(h_\kappa^*)^\top] = \delta_{\ell\kappa} \frac{Q_a^\top \Sigma_\ell Q_\star}{d} \equiv \theta_a^\ell. \quad (75)$$

Thus

$$\begin{aligned} \mathbb{E}Z^s &= \int dmd\hat{m}d\theta d\hat{\theta}dq d\hat{q} e^{\underbrace{-d \sum_a \sum_\ell [\hat{m}_a^{\ell\top} m_a^\ell + \text{Tr}(\theta_a^\ell \hat{\theta}_a^{\ell\top})]}_{e^{sd\Psi_t}} - d \sum_\ell \sum_{1 \leq a \leq b \leq s} \text{Tr}(q_{ab}^\ell \hat{q}_{ab}^{\ell\top})} \\ &\quad \underbrace{\int \prod_{a=1}^s dQ_a e^{-\beta \sum_{a=1}^s g(Q_a) + \sum_a \sum_\ell (\sqrt{d} \hat{m}_a^{\ell\top} Q_a^\top p_\ell + \text{Tr}[\theta_a^\ell Q_\star^\top \Sigma_\ell Q_a]) + \sum_{1 \leq a \leq b \leq s} \sum_\ell \text{Tr}[q_{ab}^\ell Q_b^\top \Sigma_\ell Q_a]}_{e^{sd\Psi_Q}} \\ &\quad \underbrace{\left[\mathbb{E}_{h^\star, \{h_a\}_{a=1}^s} e^{-\beta \sum_{a=1}^s (\text{Tr} S[h^a + m^a] \rho_\Sigma S[h^a + m^a]^\top - 2 \text{Tr} T[h^\star] \rho_\Sigma S[h^a + m^a]^\top)} \right]^{\alpha d}}_{e^{s\alpha d\Psi_y}}, \end{aligned} \quad (76)$$

where we decomposed the replicated free entropy into the trace, entropic and energetic potentials Ψ_t, Ψ_Q, Ψ_y . Note that all exponents are scaling with $d \rightarrow \infty$. Therefore the integral in (76) can be computed using a Laplace saddle-point approximation.

C.1 Replica-Symmetric ansatz

We have thus rephrased the analysis of the measure (67) as a optimization problem over the order parameters $\{q_{ab}^\ell, \theta_a^\ell, m_a\}$, and the associated conjugate variables. However, these still represent $2L(s^2 + 1) + 2s$ variables, and $s \rightarrow 0$. In order to make progress, we assume that the maximizer is of *replica-symmetric* (RS) form (Parisi, 1983, 1979)

$$q_{ab}^\ell = (r_\ell - q_\ell) \delta_{ab} + q_\ell \quad (77)$$

$$m_a^\ell = m_\ell \quad (78)$$

$$\theta_a^\ell = \theta_\ell \quad (79)$$

$$\hat{q}_{ab}^\ell = -(\hat{r}_\ell/2 + \hat{q}_\ell) + \hat{q}_\ell \quad (80)$$

$$\hat{m}_a^\ell = \hat{m}_\ell \quad (81)$$

$$\hat{\theta}_a^\ell = \hat{\theta}_\ell \quad (82)$$

The RS ansatz holds in a number of machine learning settings, notably for convex problems and Bayes-optimal settings, see e.g. (Zdeborová & Krzakala, 2016) for a review. In the present setting, since the empirical loss (3) is non-convex, we emphasize that the RS ansatz constitutes a heuristic technical assumption of our analysis.

C.2 Entropic potential

We now turn to the entropic potential Ψ_w . It is convenient to introduce the variance order parameter

$$\hat{V}_\ell \equiv \hat{r}_\ell + \hat{q}_\ell. \quad (83)$$

The entropic potential can then be expressed as

$$\begin{aligned}
& e^{\beta s d \Psi_Q} \\
&= \int \prod_{a=1}^s dQ_a e^{-\beta \sum_a g(Q^a) + \sum_{\ell=1}^L \sum_{a=1}^s \left(\sqrt{d} \hat{m}_\ell^\top Q_a^\top p_\ell + \text{Tr}[\hat{Q}_\ell^\top \Sigma_\ell Q_a] \right) - \frac{1}{2} \sum_{\ell=1}^L \sum_{a=1}^s \text{Tr}[\hat{V}_\ell Q_a \Sigma_\ell Q_a^\top] + \frac{1}{2} \sum_{\ell=1}^L \sum_{a,b} \text{Tr}[\hat{q}_\ell Q_a \Sigma_\ell Q_b^\top]} \\
&= \int \prod_{\ell=1}^L D\Xi_\ell \\
&\quad \left[\int dQ e^{-\beta g(Q) - \frac{1}{2} \text{Tr} \left[\sum_{\ell=1}^L \hat{V}_\ell Q \Sigma_\ell Q^\top \right] + \left(\sum_{\ell=1}^L (\sqrt{d} \hat{m}_\ell p_\ell^\top + \hat{\theta}_\ell Q_\star^\top \Sigma_\ell) + \sum_{\ell=1}^L \Xi_\ell \odot (\hat{q}_\ell \otimes \Sigma_\ell)^{\frac{1}{2}} \right) \odot Q} \right]^s \\
&= \mathbb{E}_\Xi \left[\int dQ e^{-\beta g(Q) - \frac{1}{2} Q \odot \left[\sum_{\ell=1}^L \hat{V}_\ell \otimes \Sigma_\ell \right] \odot Q + \left(\sum_{\ell=1}^L (\sqrt{d} \hat{m}_\ell p_\ell^\top + \hat{\theta}_\ell Q_\star^\top \Sigma_\ell) + \sum_{\ell=1}^L \Xi_\ell \odot (\hat{q}_\ell \otimes \Sigma_\ell)^{\frac{1}{2}} \right) \odot Q} \right]^s. \tag{84}
\end{aligned}$$

Therefore

$$\beta \Psi_w = \frac{1}{d} \int \mathbb{E}_\Xi \ln \left[\int dQ e^{-\beta g(Q) - \frac{1}{2} Q \odot \left[\sum_{\ell=1}^L \hat{V}_\ell \otimes \Sigma_\ell \right] \odot Q + \left(\sum_{\ell=1}^L (\sqrt{d} \hat{m}_\ell p_\ell^\top + \hat{\theta}_\ell Q_\star^\top \Sigma_\ell) + \sum_{\ell=1}^L \Xi_\ell \odot (\hat{q}_\ell \otimes \Sigma_\ell)^{\frac{1}{2}} \right) \odot Q} \right]. \tag{85}$$

For a matrix $\Xi \in \mathbb{R}^{r \times d}$ and tensors $\mathbf{A}, \mathbf{B} \in \mathbb{R}^{r \times d} \otimes \mathbb{R}^{r \times d}$, we denoted $(\Xi \odot \mathbf{A})_{kl} = \sum_{ij} \Xi^{ij} \mathbf{A}_{ij,kl}$ and $(\mathbf{A} \odot \mathbf{B})_{ij,kl} = \sum_{rs} \mathbf{A}_{ij,rs} \mathbf{B}_{rs,kl}$.

C.3 Energetic potential

The computation of the energetic potential Ψ_y is rather standard and follows the same lines as in e.g. (Aubin et al., 2018), yielding

$$\begin{aligned}
\beta \Psi_y &= \int_{\mathbb{R}^{L \times t}} dY DZ \int_{\mathbb{R}^{L \times r}} D\Xi \prod_{\ell=1}^L \delta \left[y_\ell - (\rho_\ell - \theta_\ell^\top q_\ell^{-1} \theta_\ell)^{\frac{1}{2}} z_\ell - \theta_\ell^\top q_\ell^{\frac{1}{2}} \xi_\ell \right] \\
&\quad \times \ln \left[\int_{\mathbb{R}^{L \times r}} dX \prod_{\ell=1}^L \frac{e^{-\frac{1}{2} \left(x_\ell - q_\ell^{\frac{1}{2}} \xi_\ell \right)^\top V_\ell^{-1} \left(x_\ell - q_\ell^{\frac{1}{2}} \xi_\ell \right)}}{\det(2\pi V_\ell)} e^{-\beta \text{Tr} \mathbf{S}[x+m] \rho_\sigma \mathbf{S}[x+m]^\top - 2 \text{Tr} \mathbf{T}[y] \rho_\Sigma \mathbf{S}[x+m]^\top} \right] \\
&= \underbrace{\int_{\mathbb{R}^{L \times t}} dY \int_{\mathbb{R}^{L \times r}} D\Xi \prod_{\ell=1}^L \frac{e^{-\frac{1}{2} \left(y_\ell - \theta_\ell^\top q_\ell^{\frac{1}{2}} \xi_\ell \right)^\top (\rho_\ell - \theta_\ell^\top q_\ell^{-1} \theta_\ell)^{-1} \left(y_\ell - \theta_\ell^\top q_\ell^{\frac{1}{2}} \xi_\ell \right)}}{\det \left[2\pi (\rho_\ell - \theta_\ell^\top q_\ell^{-1} \theta_\ell) \right]}}_{\Xi \in \mathbb{E}_{Y, \Xi}} \\
&\quad \times \ln \left[\int_{\mathbb{R}^{L \times r}} dX \prod_{\ell=1}^L \frac{e^{-\frac{1}{2} \left(x_\ell - q_\ell^{\frac{1}{2}} \xi_\ell \right)^\top V_\ell^{-1} \left(x_\ell - q_\ell^{\frac{1}{2}} \xi_\ell \right)}}{\det(2\pi V_\ell)} e^{-\beta \text{Tr} \mathbf{S}[x+m] \rho_\sigma \mathbf{S}[x+m]^\top - 2 \text{Tr} \mathbf{T}[y] \rho_\Sigma \mathbf{S}[x+m]^\top} \right] \tag{86}
\end{aligned}$$

C.4 Zero-temperature limit

We now take the limit $\beta \rightarrow \infty$. Rescaling

$$\beta \hat{V}_\ell \leftarrow \hat{V}_\ell, \quad \frac{1}{\beta} V_\ell \leftarrow V_\ell, \quad \beta \hat{m}_\ell \leftarrow \hat{m}_\ell, \quad \beta \hat{\theta}_\ell \leftarrow \hat{\theta}_\ell, \quad \beta^2 \hat{q}_\ell \leftarrow \hat{q}_\ell \tag{87}$$

The entropic potential then reduces to

$$\Psi_w = \frac{1}{2d} \mathbb{E}_{\Xi} \text{Tr} \left[\left(\sum_{\ell=1}^L \hat{V}_\ell \otimes \Sigma_\ell \right) \odot \left(\sum_{\ell=1}^L (\sqrt{d} \hat{m}_\ell p_\ell^\top + \hat{\theta}_\ell Q_\star^\top \Sigma_\ell) + \sum_{\ell=1}^L \Xi_\ell \odot (\hat{q}_\ell \otimes \Sigma_\ell)^{\frac{1}{2}} \right)^{\otimes 2} \right] - \frac{1}{d} \mathbb{E}_{\Xi} \mathcal{M}_g(\Xi) \quad (88)$$

where we defined the entropic Moreau envelope

$$M_g(\Xi) \equiv \inf_Q \left\{ \frac{1}{2} \left\| \left(\sum_{\ell=1}^L \hat{V}_\ell \otimes \Sigma_\ell \right)^{1/2} \left(Q - \left(\sum_{\ell=1}^L \hat{V}_\ell \otimes \Sigma_\ell \right)^{-1} \left(\sum_{\ell=1}^L (\sqrt{d} \hat{m}_\ell p_\ell^\top + \hat{\theta}_\ell Q_\star^\top \Sigma_\ell) + \sum_{\ell=1}^L \Xi_\ell \odot (\hat{q}_\ell \otimes \Sigma_\ell)^{\frac{1}{2}} \right) \right\|^2 + g(Q) \right\}. \quad (89)$$

The energetic potential can be similarly recast into a more compact form

$$\Psi_y = -\mathbb{E}_{Y, \Xi} \mathcal{M}(Y, \Xi) \quad (90)$$

where the Moreau envelope is defined as

$$\mathcal{M}(Y, \Xi) = \inf_X \frac{1}{2} \left\{ \sum_{\ell=1}^L \text{Tr} \left[V_\ell^{-1} \left(x_\ell - q_\ell^{1/2} \xi_\ell - m_\ell \right)^{\otimes 2} \right] + \text{Tr} \left[\mathbf{S}(X) \rho_\Sigma \mathbf{S}(X)^\top \right] - 2 \text{Tr} \left[\mathbf{T}(Y) \rho_\Sigma \mathbf{S}(X)^\top \right] \right\}. \quad (91)$$

C.5 Replica free entropy

One finally reaches an expression for the replica free entropy as

$$\Phi = \frac{1}{2} \sum_{\ell=1}^L \left(\text{Tr} \hat{V}_\ell q_\ell - \text{Tr} \hat{q}_\ell V_\ell \right) - \sum_{\ell=1}^L \hat{m}_\ell^\top m_\ell - \sum_{\ell=1}^L \text{Tr} \hat{\theta}_\ell^\top \theta_\ell - \frac{1}{d} \mathbb{E}_{\Xi} \mathcal{M}_g(\Xi) + \frac{1}{2d} \mathbb{E}_{\Xi} \text{Tr} \left[\left(\sum_{\ell=1}^L \hat{V}_\ell \otimes \Sigma_\ell \right) \odot \left(\left(\sqrt{d} \hat{m}_\ell p_\ell^\top + \hat{\theta}_\ell Q_\star^\top \Sigma_\ell \right) + \sum_{\ell=1}^L \Xi_\ell \odot (\hat{q}_\ell \otimes \Sigma_\ell)^{\frac{1}{2}} \right)^{\otimes 2} \right] - \alpha \mathbb{E}_{y, \xi} \mathcal{M}(y, \xi) \quad (92)$$

C.6 Saddle-point equations : general regularizer

The extremization of the free entropy (92) yields, similarly to (Cui & Zdeborová, 2023), the following system of self-consistent equations on the summary statistics:

$$\begin{cases} V_\ell = \frac{1}{d} \mathbb{E}_{\Xi} \left[\left(\text{prox}_g \odot (\hat{q}_\ell \otimes \Sigma_\ell)^{-\frac{1}{2}} \odot (\mathbb{I}_r \otimes \Sigma_\ell) \right) \Xi_\ell^\top \right] \\ q_\ell = \frac{1}{d} \mathbb{E}_{\Xi} \left[\text{prox}_g \Sigma_\ell \text{prox}_g^\top \right] \\ m_\ell = \frac{1}{\sqrt{d}} \mathbb{E}_{\Xi} \left[\text{prox}_g p_\ell \right] \\ \theta_\ell = \frac{1}{\sqrt{d}} \mathbb{E}_{\Xi} \left[\text{prox}_g \Sigma_\ell Q_\star \right] \\ \hat{q}_\ell = \alpha \mathbb{E}_{\Xi, Y} V_\ell^{-1} \left(\text{prox}_\ell - q_\ell^{\frac{1}{2}} \xi_\ell - m_\ell \right)^{\otimes 2} V_\ell^{-1} \\ \hat{V}_\ell = q_\ell^{-1} \hat{\theta}_\ell \theta_\ell^\top - \alpha q_\ell^{-\frac{1}{2}} \mathbb{E}_{\Xi, Y} V_\ell^{-1} \left(\text{prox}_\ell - q_\ell^{\frac{1}{2}} \xi_\ell - m_\ell \right) \xi_\ell^\top \\ \hat{m}_\ell = \alpha \mathbb{E}_{\xi, \eta} V_\ell^{-1} \left(\text{prox}_\ell - q_\ell^{\frac{1}{2}} \xi_\ell - m_\ell \right) \\ \hat{\theta}_\ell = \alpha \mathbb{E}_{\xi, \eta} V_\ell^{-1} \left(\text{prox}_\ell - q_\ell^{\frac{1}{2}} \xi_\ell - m_\ell \right) \left(y_\ell - \xi_\ell^\top q_\ell^{-1/2} \theta_\ell \right)^\top \left(\rho_\ell - \theta_\ell^\top q_\ell^{-1} \theta_\ell \right)^{-1} \end{cases}, \quad (94)$$

where the proximals prox_g and prox_ℓ respectively refer to the arginf in Q (resp. x_ℓ) of the envelopes \mathcal{M}_g (89) (resp. \mathcal{M} 91).

C.7 Saddle-point equations : ℓ_2

We now specialize the saddle-point equations (93) to the case of an ℓ_2 regularizer $g(\cdot) = 1/2\|\cdot\|$ the entropic potential admits the simple form

$$\begin{aligned}\Psi_Q &= \frac{1}{2d} \text{Tr} \left[\left(\lambda \mathbb{I}_r \odot \mathbb{I}_d + \sum_{\ell=1}^L \hat{V}_\ell \otimes \Sigma_\ell \right)^{-1} \odot \left(\sum_{\ell=1}^L \hat{q}_\ell \otimes \Sigma_\ell + \left(\sum_{\ell=1}^L (\sqrt{d} \hat{m}_\ell p_\ell^\top + \hat{\theta}_\ell Q_\star^\top \Sigma_\ell) \right)^{\otimes 2} \right) \right] \\ &= \frac{1}{2d} \sum_{i=1}^d \text{Tr} \left[\left(\lambda + \sum_{\ell=1}^L \lambda_i^t \hat{V}_\ell \right)^{-1} \left(\sum_{\ell=1}^L \lambda_i^t \hat{q}_\ell + \left(\sum_{\ell=1}^L (\sqrt{d} \hat{m}_\ell p_\ell^\top e_i + \hat{\theta}_\ell Q_\star^\top \Sigma_\ell e_i) \right) \left(\sum_{\ell=1}^L (\sqrt{d} \hat{m}_\ell p_\ell^\top e_i + \hat{\theta}_\ell Q_\star^\top \Sigma_\ell e_i) \right)^\top \right) \right] \\ &\stackrel{d \rightarrow \infty}{\equiv} \frac{1}{2} \int d\nu(\gamma, \tau, \pi) \text{Tr} \left[\left(\lambda + \sum_{\ell=1}^L \gamma_\ell \hat{V}_\ell \right)^{-1} \left(\sum_{\ell=1}^L \gamma_\ell \hat{q}_\ell + \left(\sum_{\ell=1}^L \tau_\ell \hat{m}_\ell + \gamma_\ell \hat{\theta}_\ell \cdot \pi \right)^{\otimes 2} \right) \right].\end{aligned}\quad (95)$$

The replica free energy thus reads

$$\begin{aligned}\Phi &= \frac{1}{2} \sum_{\ell=1}^L \left(\text{Tr} \hat{V}_\ell q_\ell - \text{Tr} \hat{q}_\ell V_\ell \right) - \sum_{\ell=1}^L \hat{m}_\ell^\top m_\ell - \sum_{\ell=1}^L \text{Tr} \hat{\theta}_\ell^\top \theta_\ell - \alpha \mathbb{E}_{y, \xi} \mathcal{M}(y, \xi) \\ &\quad + \frac{1}{2} \int d\nu(\gamma, \tau, \pi) \text{Tr} \left[\left(\lambda + \sum_{\ell=1}^L \gamma_\ell \hat{V}_\ell \right)^{-1} \left(\sum_{\ell=1}^L \gamma_\ell \hat{q}_\ell + \left(\sum_{\ell=1}^L \tau_\ell \hat{m}_\ell + \gamma_\ell \hat{\theta}_\ell \cdot \pi \right)^{\otimes 2} \right) \right],\end{aligned}\quad (96)$$

leading to the saddle point equations

$$\begin{cases} \hat{q}_\ell = \alpha \mathbb{E}_{\Xi, Y} V_\ell^{-1} \left(\text{prox}_\ell - q_\ell^{\frac{1}{2}} \xi_\ell - m_\ell \right)^{\otimes 2} V_\ell^{-1} \\ \hat{V}_\ell = q_\ell^{-1} \hat{\theta}_\ell \theta_\ell^\top - \alpha q_\ell^{-\frac{1}{2}} \mathbb{E}_{\Xi, Y} V_\ell^{-1} \left(\text{prox}_\ell - q_\ell^{\frac{1}{2}} \xi_\ell - m_\ell \right) \xi_\ell^\top \\ \hat{m}_\ell = \alpha \mathbb{E}_{\xi, \eta} V_\ell^{-1} \left(\text{prox}_\ell - q_\ell^{\frac{1}{2}} \xi_\ell - m_\ell \right) \\ \hat{\theta}_\ell = \alpha \mathbb{E}_{\xi, \eta} V_\ell^{-1} \left(\text{prox}_\ell - q_\ell^{\frac{1}{2}} \xi_\ell - m_\ell \right) \left(y_\ell - \xi_\ell^\top q_\ell^{-1/2} \theta_\ell \right)^\top \left(\rho_\ell - \theta_\ell^\top q_\ell^{-1} \theta_\ell \right)^{-1} \\ q_\ell = \int d\nu(\gamma, \tau, \pi) \gamma_\ell \left(\lambda \mathbb{I}_r + \sum_{\kappa=1}^L \gamma_\kappa \hat{V}_\kappa \right)^{-2} \left(\sum_{\kappa=1}^L \gamma_\kappa \hat{q}_\kappa + \left(\sum_{\kappa=1}^L \hat{m}_\kappa \tau_\kappa + \gamma_\kappa \hat{\theta}_\kappa \cdot \pi \right)^{\otimes 2} \right) \\ V_\ell = \int d\nu(\gamma, \tau, \pi) \gamma_\ell \left(\lambda \mathbb{I}_r + \sum_{\kappa=1}^L \gamma_\kappa \hat{V}_\kappa \right)^{-1} \\ m_\ell = \int d\nu(\gamma, \tau, \pi) \tau_\ell \left(\lambda \mathbb{I}_r + \sum_{\kappa=1}^L \gamma_\kappa \hat{V}_\kappa \right)^{-1} \left(\sum_{\kappa=1}^L \hat{m}_\kappa \tau_\kappa + \gamma_\kappa \hat{\theta}_\kappa \cdot \pi \right) \\ \theta_\ell = \int d\nu(\gamma, \tau, \pi) \gamma_\ell \left(\lambda \mathbb{I}_r + \sum_{\kappa=1}^L \gamma_\kappa \hat{V}_\kappa \right)^{-1} \left(\sum_{\kappa=1}^L \hat{m}_\kappa \tau_\kappa + \gamma_\kappa \hat{\theta}_\kappa \cdot \pi \right) \pi^\top. \end{cases}\quad (97)$$

which finishes to recover (7). Let us finally mention that the update equations (7) for the summary statistics (6) do *not* describe the dynamics of gradient descent, but rather that of an Approximate Message Passing algorithm (Bayati & Montanari, 2011a), which we elicit in Appendix B for completeness. \square

C.8 test MSE

The generalization performance is measured by the test error

$$\epsilon_g \equiv \mathbb{E}_{\mathcal{D}} \mathbb{E}_x \left\| \text{T} \left[\frac{1}{\sqrt{d}} x Q_\star \right] x - \text{S} \left[\frac{1}{\sqrt{d}} (x+p) \hat{Q} \right] (x+p) \right\|^2. \quad (98)$$

Expliciting this expression in terms of the correlated Gaussian variables xQ_* , xQ allows to straightforwardly show that ϵ_g admits the sharp asymptotic characterization in terms of the summary statistics characterized by (97):

$$\epsilon_g = \mathbb{E}_X \text{Tr} \left[\mathbf{S}[X] \rho_\Sigma \mathbf{S}[X]^\top \right] + \mathbb{E}_Y \text{Tr} \left[\mathbf{T}[Y] \rho_\Sigma \mathbf{T}[Y]^\top \right] - 2 \mathbb{E}_{X,Y} \text{Tr} \left[\mathbf{S}[X] \rho_\Sigma \mathbf{T}[Y]^\top \right], \quad (99)$$

where the average bears on $X \in \mathbb{R}^{L \times r}$, $Y \in \mathbb{R}^{L \times t}$ with independent rows with statistics

$$(x_\ell, y_\ell) \sim \mathcal{N} \left[\begin{pmatrix} m \\ 0 \end{pmatrix}, \begin{pmatrix} q_\ell & \theta_\ell \\ \theta_\ell^\top & \rho_\ell \end{pmatrix} \right] \quad (100)$$

C.9 Training loss

We finally turn to the training loss. It is reasonable to expect, from statistical physics, that the training loss should be equal to the free energy $-\Phi$ at zero temperature. We provide below an alternative derivation, for simplicity in the case of ℓ_2 regularization $g = 1/2 \|\cdot\|^2$. First note that the training loss ϵ_t can be expressed as

$$\epsilon_t = - \lim_{\beta \rightarrow \infty} \partial_\beta \underbrace{\frac{1}{d} \ln Z(\beta)}_{\Phi(\beta)} \quad (101)$$

Where $\Phi(\beta)$ is the free entropy at finite temperature. The trace potential Ψ_t bears no explicit dependence on β . On the other hand,

$$\begin{aligned} \beta \Psi_Q &= -\frac{1}{2} \ln \det \left[\beta \lambda \mathbb{I}_r \otimes \mathbb{I}_d + \sum_{\ell=1}^L \hat{V}_\ell \otimes \Sigma_\ell \right] \\ &+ \frac{1}{2d} \text{Tr} \left[\left(\beta \lambda \mathbb{I}_r \odot \mathbb{I}_d + \sum_{\ell=1}^L \hat{V}_\ell \otimes \Sigma_\ell \right)^{-1} \odot \left(\sum_{\ell=1}^L \hat{q}_\ell \otimes \Sigma_\ell + \left(\sum_{\ell=1}^L (\sqrt{d} \hat{m}_\ell p_\ell^\top + \hat{\theta}_\ell Q_\star^\top \Sigma_\ell) \right)^{\otimes 2} \right) \right] \end{aligned} \quad (102)$$

Thus

$$\begin{aligned} \partial_\beta(\beta \Psi_Q) &= -\frac{\lambda}{2} \text{Tr} \left[\beta \lambda \mathbb{I}_r \otimes \mathbb{I}_d + \sum_{\ell=1}^L \hat{V}_\ell \otimes \Sigma_\ell \right]^{-1} \\ &- \frac{\lambda}{2d} \text{Tr} \left[\left(\beta \lambda \mathbb{I}_r \odot \mathbb{I}_d + \sum_{\ell=1}^L \hat{V}_\ell \otimes \Sigma_\ell \right)^{-2} \odot \left(\sum_{\ell=1}^L \hat{q}_\ell \otimes \Sigma_\ell + \left(\sum_{\ell=1}^L (\sqrt{d} \hat{m}_\ell p_\ell^\top + \hat{\theta}_\ell Q_\star^\top \Sigma_\ell) \right)^{\otimes 2} \right) \right] \end{aligned} \quad (103)$$

Finally, going through the same rescaling steps to take the $\beta \rightarrow \infty$ limit,

$$\lim_{\beta \rightarrow \infty} \partial_\beta(\beta \Psi_Q) = -\frac{\lambda}{2d} \text{Tr} \left[\left(\lambda \mathbb{I}_r \odot \mathbb{I}_d + \sum_{\ell=1}^L \hat{V}_\ell \otimes \Sigma_\ell \right)^{-2} \odot \left(\sum_{\ell=1}^L \hat{q}_\ell \otimes \Sigma_\ell + \left(\sum_{\ell=1}^L (\sqrt{d} \hat{m}_\ell p_\ell^\top + \hat{\theta}_\ell Q_\star^\top \Sigma_\ell) \right)^{\otimes 2} \right) \right] \quad (104)$$

By the same token, it is straightforward to see that

$$\lim_{\beta \rightarrow \infty} \partial_\beta(\beta \Psi_y) = -\mathbb{E}_{Y, \Xi} \left[\mathcal{M}(Y, \Xi) - \frac{1}{2} \sum_{\ell=1}^L \text{Tr} \left[\underbrace{V_\ell^{-1} \left(x_\ell - q_\ell^{1/2} \xi_\ell - m_\ell \right)^{\otimes 2}}_{\hat{q}_\ell V_\ell} \right] \right] \quad (105)$$

We used the self-consistent equations (7) to identify the term in underbrace. Putting everything together,

$$\begin{aligned}
-\epsilon_t &= \lim_{\beta \rightarrow \infty} \partial_\beta \Psi(\beta) = -\frac{\lambda}{2} \int d\nu(\gamma, \tau) \operatorname{Tr} \left[\left(\lambda + \sum_{\ell=1}^L \gamma_\ell \hat{V}_\ell \right)^{-1} \left(\sum_{\ell=1}^L \gamma_\ell \hat{q}_\ell + \left(\sum_{\ell=1}^L \tau_\ell \hat{m}_\ell + \hat{\theta}_\ell \cdot \pi \right)^{\otimes 2} \right) \right] \\
&\quad - \alpha \mathbb{E}_{Y, \Xi} [\mathcal{M}(Y, \Xi)] + \frac{1}{2} \sum_{\ell=1}^L \operatorname{Tr}[\hat{q}_\ell V_\ell].
\end{aligned} \tag{106}$$

This constitutes a sharp asymptotic characterization of the training loss ϵ_t as a function of the summary statistics characterized in Result 4.2.

For completeness, we finally explicit the connection between ϵ_t and the negative free entropy (i.e. the *free energy* in statistical physics). We go back to massage the expression for the free entropy

$$\begin{aligned}
\Phi &= \frac{1}{2} \sum_{\ell=1}^L \left(\operatorname{Tr} \hat{V}_\ell q_\ell - \operatorname{Tr} \hat{q}_\ell V_\ell \right) - \sum_{\ell=1}^L \hat{m}_\ell^\top m_\ell - \sum_{\ell=1}^L \operatorname{Tr} \hat{\theta}_\ell^\top \theta_\ell - \alpha \mathbb{E}_{Y, \Xi} \mathcal{M}(Y, \Xi) \\
&\quad + \frac{1}{2} \int d\nu(\gamma, \tau) \operatorname{Tr} \left[\left(\lambda + \sum_{\ell=1}^L \gamma_\ell \hat{V}_\ell \right)^{-1} \left(\sum_{\ell=1}^L \gamma_\ell \hat{q}_\ell + \left(\sum_{\ell=1}^L \tau_\ell \hat{m}_\ell + \gamma_\ell \hat{\theta}_\ell \cdot \pi \right)^{\otimes 2} \right) \right] \\
&= \frac{1}{2} \sum_{\ell=1}^L \operatorname{Tr} [\hat{q}_\ell V_\ell + \hat{V}_\ell q_\ell] - \frac{1}{2} \int d\nu(\gamma, \tau) \operatorname{Tr} \left[\left(\lambda + \sum_{\ell=1}^L \gamma_\ell \hat{V}_\ell \right)^{-1} \left(\sum_{\ell=1}^L \gamma_\ell \hat{q}_\ell + \left(\sum_{\ell=1}^L \tau_\ell \hat{m}_\ell + \gamma_\ell \hat{\theta}_\ell \cdot \pi \right)^{\otimes 2} \right) \right] \\
&\quad - \alpha \mathbb{E}_{Y, \Xi} \mathcal{M}(Y, \Xi) \\
&= \frac{1}{2} \sum_{\ell=1}^L \operatorname{Tr} [\hat{q}_\ell V_\ell] + \frac{1}{2} \int d\nu(\gamma, \tau) \operatorname{Tr} \left[\left(\lambda + \sum_{\ell=1}^L \gamma_\ell \hat{V}_\ell \right)^{-2} \left(\sum_{\ell=1}^L \hat{V}_\ell \gamma_\ell - \lambda - \sum_{\ell=1}^L \gamma_\ell \hat{V}_\ell \right) \left(\sum_{\ell=1}^L \gamma_\ell \hat{q}_\ell + \left(\sum_{\ell=1}^L \tau_\ell \hat{m}_\ell + \gamma_\ell \hat{\theta}_\ell \cdot \pi \right)^{\otimes 2} \right) \right] \\
&\quad - \alpha \mathbb{E}_{Y, \Xi} \mathcal{M}(Y, \Xi) \\
&= -\frac{\lambda}{2} \int d\nu(\gamma, \tau) \operatorname{Tr} \left[\left(\lambda + \sum_{\ell=1}^L \gamma_\ell \hat{V}_\ell \right)^{-1} \left(\sum_{\ell=1}^L \gamma_\ell \hat{q}_\ell + \left(\sum_{\ell=1}^L \tau_\ell \hat{m}_\ell + \hat{\theta}_\ell \cdot \pi \right)^{\otimes 2} \right) \right] \\
&\quad - \alpha \mathbb{E}_{Y, \Xi} [\mathcal{M}(Y, \Xi)] + \frac{1}{2} \sum_{\ell=1}^L \operatorname{Tr}[\hat{q}_\ell V_\ell] \\
&= -\epsilon_t
\end{aligned} \tag{107}$$

In other words, the training loss is equal to the zero-temperature free energy.

D Derivation of Result 5.1

In this Appendix we derive the asymptotic characterization of the learning performance of the dense linear baseline (15), as stated in Result 5.1. Consider the empirical risk minimization (16)

$$\mathcal{R}(W) = \frac{1}{n} \sum_{\mu=1}^n \|A^*(x^\mu) x^\mu - W x^\mu\|^2 \tag{108}$$

where we use the shorthand notation $A^*(x) \equiv \mathbb{T}[1/\sqrt{dx}Q_\star]$ for the target attention score matrix (1). The expression for the risk can be asymptotically simplified as

$$\begin{aligned}\mathcal{R}(W) &= \frac{1}{n} \sum_{\mu=1}^n \left[A^*(x^\mu) \rho_\Sigma A^*(x^\mu)^\top - (A^*(x^\mu) \rho_\Sigma W^\top + \text{h.c.}) + W \rho_\Sigma W^\top + o(1/\sqrt{d}) \right] \\ &\approx \mathbb{E}_x \left[A^*(x) \rho_\Sigma A^*(x)^\top \right] - (W \rho_\Sigma \mathbb{E}_x [A^*(x)]^\top + \text{h.c.}) + W \rho_\Sigma W^\top \\ &= \mathbb{E}_x \left[A^*(x) \rho_\Sigma A^*(x)^\top \right] - \mathbb{E}_x [A^*(x)] \rho_\Sigma \mathbb{E}_x [A^*(x)]^\top + \left\| \rho_\Sigma^{1/2} \left(W - \mathbb{E}_x [A^*(x)] \right) \right\|^2\end{aligned}\quad (109)$$

Therefore the learnt weight \hat{W} is simply equal to

$$\hat{W} = \mathbb{E}_x [A^*(x)] = \mathbb{E}_x [\mathbb{T}[1/\sqrt{dx}Q_\star]]. \quad (110)$$

Naming $h = 1/\sqrt{dx}Q_\star$ the argument of the last term, the matrix h possesses independent rows with statistics

$$h_\ell \sim \mathcal{N}(0, \rho_\ell) \quad (111)$$

where we remind that $\rho_\ell \equiv 1/dQ_\star^\top \Sigma_\ell Q_\star$. Therefore, the trained weights \hat{W} obtained by minimizing the *empirical* loss also coincide with the minimizer of the *population* loss. Intuitively, this follows from the fact that in the asymptotic limit considered $n, d \rightarrow \infty$ and $L = \Theta_d(1)$, training W , i.e. a number $L^2 = \Theta_d(1)$ of parameters on the empirical loss for $n \ll L^2$ data points is equivalent asymptotically to directly training on the population loss. Expliciting the corresponding test MSE, one reaches the sharp asymptotic characterization

$$\begin{aligned}\epsilon_g^{\text{lin}} &= \frac{1}{L} \text{Tr} [\hat{W} \rho_\Sigma \hat{W}^\top] + \frac{1}{L} \mathbb{E}_h \text{Tr} [\mathbb{T}[h] \rho_\Sigma \mathbb{T}[h]^\top] \\ &\quad - \frac{2}{L} \mathbb{E}_h \text{Tr} [\hat{W} \rho_\Sigma \mathbb{T}[h]^\top].\end{aligned}\quad (112)$$

We close this Appendix by giving a few examples for definiteness.

D.1 Examples

Purely positional target Let us consider the case where the target is purely positional, i.e. $\mathbb{T}[x] = A$ for all x . This corresponds to the $\omega = 1$ limit of the target (14). It then follows from Result 5.1 that the dense linear layer recover perfectly the target weights $\hat{W} = A$.

Target (14) For the target discussed in the main text (14),

$$\hat{W} = (1 - \omega) \mathbb{E}_h \text{softmax}(hh^\top) + \omega A \quad (113)$$

with h and having independent rows $h_\ell \sim \mathcal{N}(0, \rho_\ell)$.

E Supplementary Experiments

E.1 Empirical scaling of $\alpha = d/n$

In the following we verify that our experiments are consistent with the scaling behaviour predicted from the theory. We jointly increase d and n for a fixed value of α . In Fig. 7 we indeed observe the expected behaviour for an exemplary value of $\alpha = 2$. The same holds for the summary statistics θ and m , which concentrate as d and n jointly grow, shown in Fig. 8.

E.2 Alternative hyperparameters

We provide supplementary results for different parameter settings. Fig. 9 on the left shows more slices from the phase diagram that appears in the main Fig. 4. For the experimental section of the main text, we chose a specific A for definiteness. In the following, we present the same results for a different A with a stronger off-diagonal and a higher rank,

$$A = \begin{pmatrix} 0.3 & 0.7 \\ 0.8 & 0.2 \end{pmatrix}. \quad (114)$$

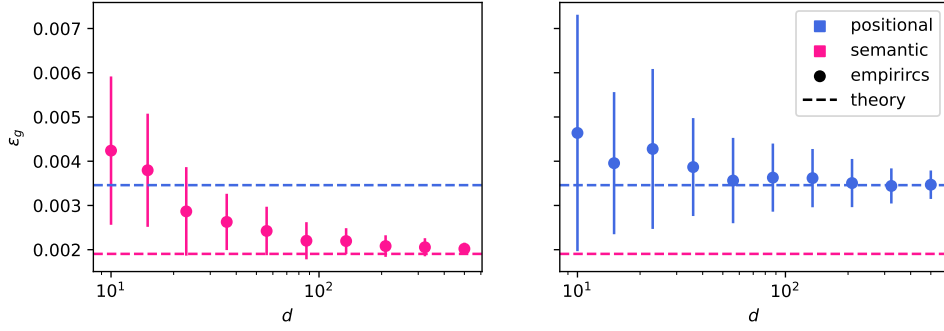


Figure 7: Scaling d and n jointly for $\alpha = 1.5$ approaches the theoretical prediction of the generalization error of the positional and semantic local minima. Experimental settings as in Fig. 2, with 70 runs per datapoint.

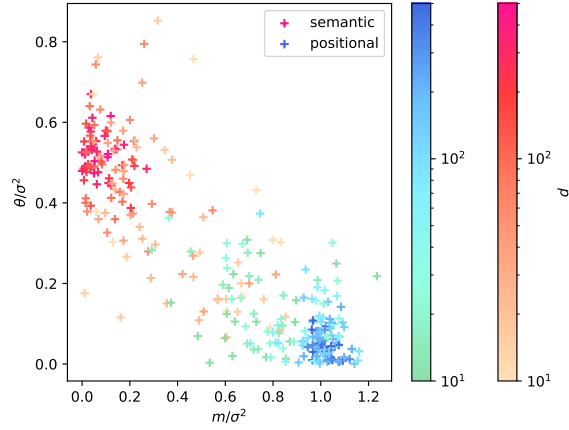


Figure 8: Scaling d and n jointly for $\alpha = 1.5$ approaches concentrates for θ and m , in different locations for the positional and semantic local minima each. Experimental settings as in Fig. 2. We show 30 runs for each $d \in [10, 15, 23, 36, 56, 87, 135, 209, 323, 500]$.

In Fig. 10 we present the analogous simulations to Fig. 3 & 4. While the global phenomena match the previous example, the details of the transitions location differ. Finally, we show the crossover for a student with higher capacity, i.e. $r_s = 2$. We show that the phenomenology remains the same in Fig. 11. However, the crossover happens at larger α – in order to make use of the dot-product attention over the linear we need comparatively more data (but since $r_s = 2$ rather than 1, we also have a factor 2 of more parameters to learn).

E.3 Uninformed initialization and training via Adam

In our experiments, to obtain the empirical results, we initialize the GD optimizer in an informed fashion, i.e. initializing Q_* of the student with $r = 1$ as either p_1 (positional) or Q_* (semantics). GD then converges in the two local optima described by our theory.

Since our theory only ascertains that these solutions predicted are indeed fixed points of GD for large sizes, this does not have direct implications for other types of optimization algorithms. In Fig. 12 we show that indeed running the Adam optimizer from an *uninformed* initialization may lead one to either of the local minima for $d = 100$. For larger d we observe the semantic minimum is reached less often than the positional minimum, and a considerable number of times the algorithm simply does not find either of them.

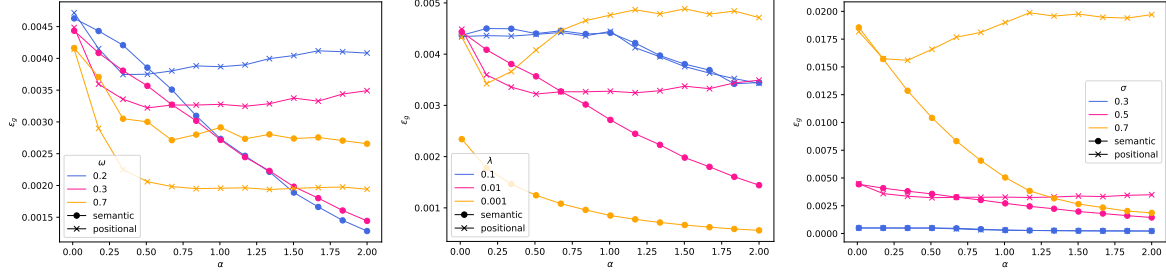


Figure 9: *Alternative Parameters*. Mixed positional/semantic teacher for $\omega = 0.3$. Settings is $r_s = r_t = 1, L = 2, A = ((0.6, 0.4), (0.4, 0.6)), \Sigma_1 = \Sigma_2 = 0.25\mathbb{I}_d, \mathbf{p}_1 = \mathbf{1}_d = -\mathbf{p}_2$ and $\mathbf{Q}_* \sim \mathcal{N}(0, \mathbb{I}_d)$. While keeping all other settings the same, we vary from left to right: The target positionality ω , the student regularizer λ and the standard deviation σ (which is $0.5 = \sqrt{\Sigma_1}$). Experiment settings as in Fig. 2.

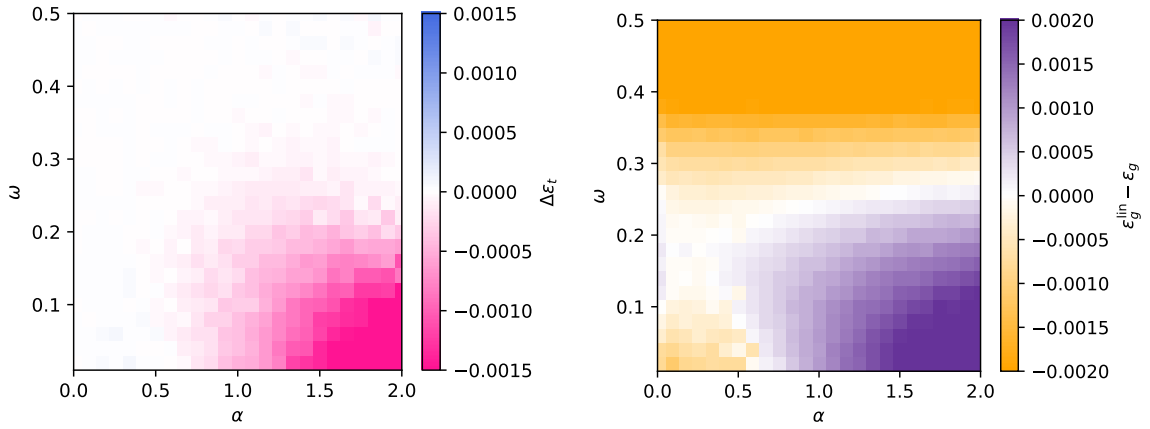


Figure 10: *Alternative Positional Matrix*. $r_s = r_t = 1, L = 2, \Sigma_1 = \Sigma_2 = 0.25\mathbb{I}_d, \mathbf{p}_1 = -\mathbf{p}_2$ and $\mathbf{p}_1, \mathbf{Q}_* \sim \mathcal{N}(0, \mathbb{I}_d)$ independently. Here, we use a definite matrix A from (114), which differs from the one used in the main text. Experiments were conducted as in Fig. 2.

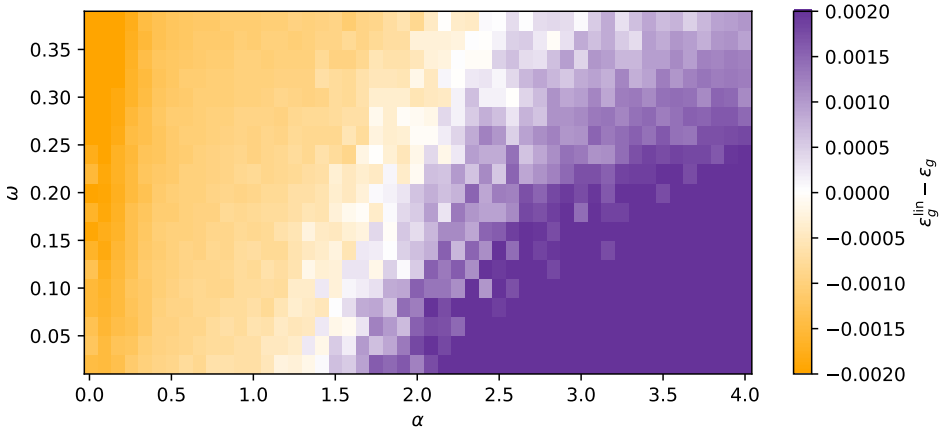


Figure 11: *Higher capacity student*. $r_s = 2, r_t = 1, L = 2, \Sigma_1 = \Sigma_2 = 0.25\mathbb{I}_d, \mathbf{p}_1 = -\mathbf{p}_2$ and $\mathbf{p}_1, \mathbf{Q}_* \sim \mathcal{N}(0, \mathbb{I}_d)$. Here, for the higher rank student, we show the average of 10 runs of GD on an *uninformed* initialization (rather than informed as in all our previous experiments, e.g. Fig. 2). We observe that in the case of $r_s = 2$ no informed initialization is necessary to outperform the linear model.

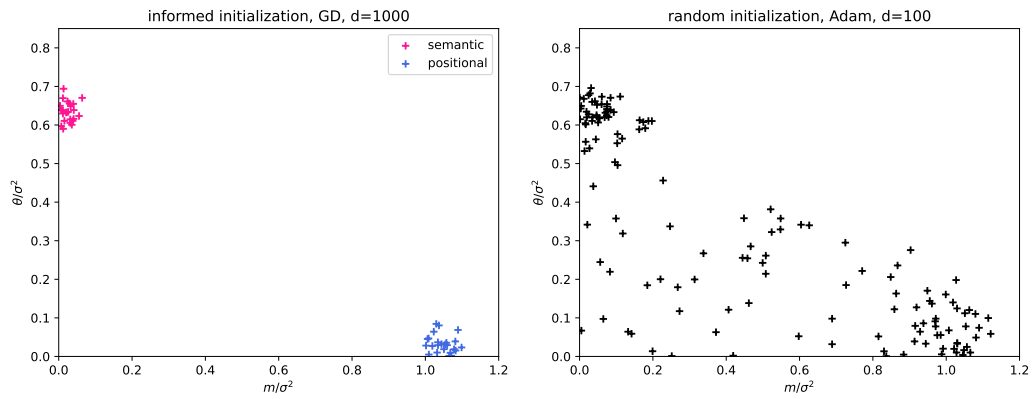


Figure 12: *Comparing GD and Adam*. Settings as in Fig. 2 for the sample complexity $\alpha = 2$. The student parameter \mathbf{Q} is obtained via either **(left)** positional and semantic informed initialization and **(right)** GD training from a random initialization are compared. Each point represents a single run. For the informed GD, we used the same optimization parameters as in Fig. 2 (24 runs per initialization). For Adam we trained on the same data, but for 2,500 epochs with learning rate $\eta = 0.01$ (showing 140 runs).